The Astrophysical Journal, 756:33 (19pp), 2012 September 1 doi:10.1088/0004-637X/756/1/33


# *CHANDRA* X-RAY OBSERVATIONS OF THE TWO BRIGHTEST UNIDENTIFIED HIGH GALACTIC LATITUDE *FERMI*-LAT $\gamma$-RAY SOURCES

C. C. Cheung[1,2,8], D. Donato[3,4], N. Gehrels[2], K. V. Sokolovsky[5,6], and M. Giroletti[7]
[1] National Research Council Research Associate, National Academy of Sciences, Washington, DC 20001, USA; Teddy.Cheung.ctr@nrl.navy.mil
[2] NASA Goddard Space Flight Center, Greenbelt, MD 20771, USA
[3] Center for Research and Exploration in Space Science and Technology (CRESST) and NASA Goddard Space Flight Center, Greenbelt, MD 20771, USA; Davide.Donato-1@nasa.gov
[4] Department of Physics and Department of Astronomy, University of Maryland, College Park, MD 20742, USA
[5] Astro Space Center of the Lebedev Physical Institute, 117810 Moscow, Russia
[6] Sternberg Astronomical Institute of the Moscow State University, 119992 Moscow, Russia
[7] INAF-Istituto di Radioastronomia, I-40129 Bologna, Italy
*Received 2012 February 21; accepted 2012 July 4; published 2012 August 10*

## ABSTRACT

We present *Chandra* ACIS-I X-ray observations of 0FGL J1311.9−3419 and 0FGL J1653.4−0200, the two brightest high Galactic latitude ($|b| > 10°$) $\gamma$-ray sources from the three-month *Fermi* Large Area Telescope (LAT) bright source list that are still unidentified. Both were also detected previously by EGRET, and despite dedicated multi-wavelength follow-up, they are still not associated with established classes of $\gamma$-ray emitters like pulsars or radio-loud active galactic nuclei. X-ray sources found in the ACIS-I fields of view are cataloged, and their basic properties are determined. These are discussed as candidate counterparts to 0FGL J1311.9−3419 and 0FGL J1653.4−0200, with particular emphasis on the brightest of the 9 and 13 *Chandra* sources detected within the respective *Fermi*-LAT 95% confidence regions. Further follow-up studies, including optical photometric and spectroscopic observations, are necessary to identify these X-ray candidate counterparts in order to ultimately reveal the nature of these enigmatic $\gamma$-ray objects.

*Key words:* galaxies: active – gamma rays: general – pulsars: general – X-rays: general

*Online-only material:* color figures

## 1. INTRODUCTION

Since its launch in 2008, the *Fermi* Large Area Telescope (LAT; Atwood et al. 2009) has enabled substantial progress in our understanding of the high-energy (HE; > 100 MeV) $\gamma$-ray universe. A long-standing problem in the field has been in the secure identification of discrete HE $\gamma$-ray sources, with most objects detected previously by COS B (Swanenburg et al. 1981) and EGRET (Hartman et al. 1999; Casandjian & Grenier 2008) remaining unidentified prior to the present *Fermi*-era. These sources have eluded identification mainly due to high source confusion in the poorly localized $\gamma$-ray regions with typical 95% confidence radii, $r_{95} \sim 0.^{\circ}4$–$0.^{\circ}7$ in the 3rd EGRET catalog (3EG; Hartman et al. 1999). Also, for variable HE emitters (e.g., Tavani et al. 1997; Nolan et al. 2003), there was a lack of prompt response to the $\gamma$-ray events, with much of the multi-wavelength follow-up work pursued many years later (e.g., Paredes et al. 2008).

Multi-wavelength follow-up observations of unidentified 3EG sources attracted much effort, but met with mixed success (see Mukherjee & Halpern 2004, for a summary). The LAT's all-sky monitoring capability (20% of the sky at all times), its increased sensitivity (>10× better than EGRET), and dramatically improved localizations over EGRET, has enabled many of the unidentified EGRET sources to be successfully associated with lower-energy counterparts. The dominant $\gamma$-ray-emitting population consists of radio-loud active galactic nuclei (AGNs), including blazars and radio galaxies. Perhaps unexpectedly, a substantial population of new $\gamma$-ray pulsars have been identified ($\gamma$-ray pulsations detected via a blind search or using known radio ephemerides), along with a handful of pulsar wind nebula, supernova remnants, and $\gamma$-ray binaries. While the population of EGRET unidentified sources has quickly diminished, the number of fainter unidentified *Fermi*-LAT $\gamma$-ray objects has been increasing (see Nolan et al. 2012, for a summary).

As part of a systematic study of *Fermi*-LAT unidentified sources in X-rays, including *Suzaku* (e.g., Maeda et al. 2011; Takahashi et al. 2012), *Swift* (Falcone et al. 2011), and *XMM-Newton* (e.g., Wolff et al. 2010), we obtained new *Chandra* observations in cycle-11 covering the fields of five unidentified high Galactic latitude sources from the initial three-month *Fermi*-LAT bright source list (0FGL; Abdo et al. 2009a). With its large field of view (FOV; $17' \times 17'$, sufficient to cover the LAT 95% confidence regions completely) and excellent sensitivity ($5\sigma$ flux sensitivity of $\sim 1.5 \times 10^{-14}$ erg s$^{-1}$ cm$^{-2}$, 0.5–8 keV), *Chandra* observations allow for a sensitive study of all X-ray sources within the LAT localization regions. For the three targets subsequently identified as pulsars, PSR J2214+3002/0FGL J2214.8+3002 (Ransom et al. 2011) and PSR J2241−5236/0FGL J2241.7−5239 (Keith et al. 2011), and a possible radio-quiet millisecond pulsar (MSP) in 0FGL J2339.8−0530 (Kong et al. 2012), we reported the results of our *Chandra* observations in those papers. Here, we present the results of the *Chandra* study of the remaining two objects (0FGL J1311.9−3419 and 0FGL J1653.4−0200).[9] These *Fermi*-LAT sources were detected previously by EGRET, as 3EG J1314−3431/EGR J1314−3417 and 3EG J1652−0223/EGR J1653−0249 (Hartman et al. 1999; Casandjian & Grenier 2008), and are two of the brightest remaining unidentified sources from that era.

[8] Resident at Naval Research Laboratory, Washington, DC 20375, USA.

[9] Throughout, we retain the 0FGL names although newer information, particularly from the 2FGL release, are used. For reference, the various *Fermi*-LAT catalog names for the sources studied in this paper are 0FGL J1311.9−3419 = 1FGL J1311.7−3429 = 2FGL J1311.7−3429 and 0FGL J1653.4−0200 = 1FGL J1653.6−0158 = 2FGL J1653.6−0159.

**Table 1**
*Chandra* Observational Summary for the Two Targets

| Name | Pointing Center | | LAT Centroid | | ObsID | Start Time | Net Exp. |
|---|---|---|---|---|---|---|---|
| | R.A. | Decl. | $l$ (deg) | $b$ (deg) | | in 2010 (UT) | (ks) |
| 0FGL J1311.9−3419 | 13 11 49.68 | −34 29 31.2 | 307.686 | +28.195 | 11790 | Mar 21 15:38:54 | 19.87 |
| 0FGL J1653.4−0200 | 16 53 43.68 | −01 58 30.0 | 16.593 | +24.931 | 11787 | Jan 24 06:21:27 | 20.77 |

**Notes.** The positions are the pointing centers (J2000.0 equinox) set at the time of the observations and the LAT centroids are the 2FGL catalog values in Galactic coordinates. The *Chandra* observation ID (ObsID), start time, and net exposure (Net Exp.) are also provided.

In the following, we describe the analysis of the *Chandra* observations in Section 2, including the X-ray detection and characterization methods (Section 2.1) and a more detailed analysis and discussion of individual X-ray sources found within and near the LAT localization regions (Section 2.2). Results from a search for positional matches with archival optical, near-infrared, mid-infrared, and radio catalogs are also summarized in Section 2.2. We then discuss the general population of X-ray sources as potential counterparts to the $\gamma$-ray objects with particular emphasis on the aforementioned brightest *Chandra* sources (Section 3), and conclude with a summary of the results (Section 4).

## 2. *CHANDRA* X-RAY OBSERVATIONS

We obtained *Chandra X-Ray Observatory* observations of the two targets in early 2010 with ∼20 ks exposures each (Table 1). At the time of the observational planning, the available LAT localization errors based on three months of data ($r_{95} = 12\farcm2$ and $9\farcm5$; Abdo et al. 2009a) and from an internal *Fermi*-LAT team analysis of six months of data ($r_{95} \sim 4'$–$5'$) were still relatively large. We thus opted for the larger FOV provided by the ACIS-I detector (∼$17' \times 17'$) over ACIS-S (∼$8' \times 8'$) to ensure sufficient coverage of the LAT error regions. With the currently available analysis of two years of LAT data from the 2FGL catalog (Nolan et al. 2012), the localization errors have since improved to $r_{95} \simeq 2\farcm0$ for 0FGL J1311.9−3419 (Figure 1) and $\simeq 3\farcm6$ for 0FGL J1653.4−0200 (Figure 2), and we utilize these values for the remainder of this paper.

The observations were obtained in FAINT mode at the nominal ACIS-I aim point centered toward the corner of one (I3) of its four 2×2 arrayed CCDs. The default dithering mode of *Chandra* observations enables exposure in the gaps between the CCDs, but obviously with decreased effective area. In this context, the brightest *Chandra* source (CXOU J131145.7−343030) within the 2FGL error ellipse of 0FGL J1311.9−3419 fell in such a gap. This resulted in a smaller effective area at its position (∼215 cm$^2$ at 1.5 keV compared with the maximum value of ∼500 cm$^2$ in the field; see Section 2.1 and the Appendix), thus decreasing its observed count rate and statistics for temporal and spectral analysis (Section 2.2).

### 2.1. Analysis of the ACIS-I Fields

For the analysis, we used the CIAO software (Fruscione et al. 2006) version 4.2, with updated calibration files from CALDB version 4.2.2, and the `ACIS Extract` (Broos et al. 2010) software version 2010-02-26. The data were downloaded from the *Chandra* data archive and reprocessed from the level 1 (evt1) files following the standard CIAO procedure: (1) we created a new ACIS bad pixel file using `acis_run_hotpix`, (2) we ran `acis_process_events` to create a new evt1 file with the calibration applied, (3) we identified afterglows (cosmic-ray residual events) in the CCDs using `acis_detect_afterglow`, and (4) we filtered the data on grade, status, and good time, generating two level 2 (evt2) files following the recipe of Broos et al. (2010, Appendix A therein). In the last step, a more aggressive afterglow cleaning was applied to one evt2 file for the source detection, while less aggressive afterglow cleaning was applied to the second for the actual source extraction and analysis. We checked the evt2 files for background flares and none were detected.

To search for candidate X-ray sources over the four ACIS-I chips covering each field, we ran `wavdetect` in the full energy band (0.5–8 keV) and in the two sub-bands, 0.5–2 keV (soft) and 2–8 keV (hard), using images binned by 0.5, 1, and 2 ACIS pixels ($0\farcs492$ pixel$^{-1}$). The resultant source lists found in each run were merged to produce a single master list. We then used `ACIS Extract` to excise insignificant candidate sources, to scan for sources containing afterglow events, to refine the source positions, and to perform photometric, spectral, and temporal analysis.

For both targets, 97 total sources were found in our analysis of each of the two ACIS-I fields and the complete source lists are tabulated in Appendix A. Included in the tables are the source identifiers in the form of a catalog number ($N$; ordered from increasing R.A.) and a CXOU J2000.0 coordinate based name, source positions (R.A. and decl. in J2000.0) and corresponding errors ($r$, statistical only).[10] The catalog numbers of the X-ray sources in the central $12' \times 12'$ portion of the *Chandra* images are marked in Figures 1 (0FGL J1311.9−3419) and 2 (0FGL J1653.4−0200). We also provide the source distance from the *Chandra* aim point, the effective area at 1.5 keV, net X-ray counts in each of the 0.5–8 keV, 0.5–2 keV, and 2–8 keV energy ranges, along with their respective source significances in standard deviations ($\sigma$) and probabilities ($P_B$) determined by `ACIS Extract` for the null source hypothesis. To gauge variability, a one-sample Kolmogorov–Smirnov (KS) statistic was used to calculate the probability, $P_{K-S}$, for the null hypothesis of a uniform flux for all sources. Following Broos et al. (2010), we identify five X-ray sources in each of the two fields to be possibly variable ($0.005 < P_{K-S} < 0.05$), and the remaining show no evidence for variability ($P_{K-S} > 0.05$); see Appendix A for details. One of the possibly variable sources is located within the 2FGL 95% localization of 0FGL J1653.4−0200 (Section 2.2), while the rest are positioned outside of the 95% confidence ellipses.

In order to discuss the most likely candidate X-ray counterparts to the unidentified $\gamma$-ray sources, we consider only

[10] Comparing our list of X-ray sources with USNO B1.0 catalog matches, we found a negligible offset in the 0FGL J1311.9−3419 field positions, but a systematic offset of $0\farcs52 \pm 0\farcs39$ in the 0FGL J1653.4−0200 field positions (see Appendix B for details). This is within the expected systematic uncertainty of $0\farcs6$ in *Chandra*'s astrometry (see http://cxc.harvard.edu/cal/ASPECT/celmon/), which, when considering absolute positional errors, should be added in quadrature with the statistical values.

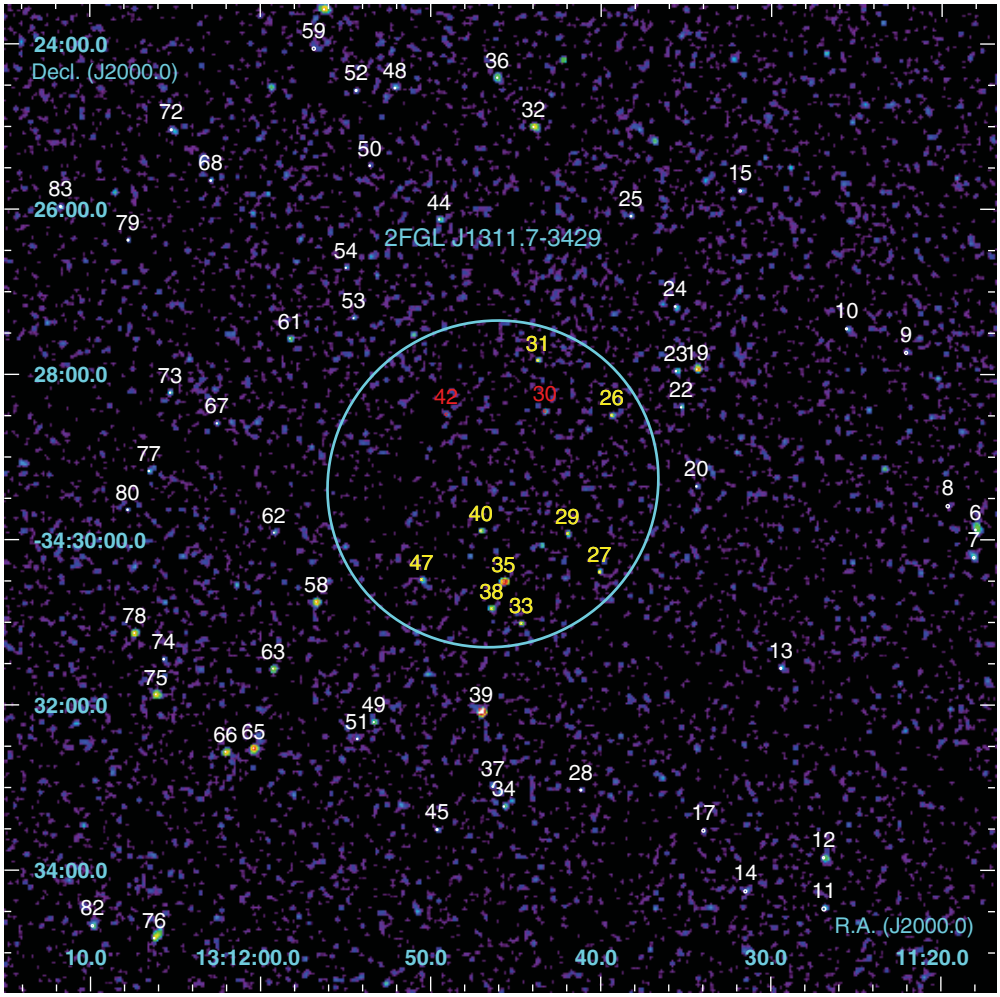


**Figure 1.** *Chandra* ACIS-I image of the central 12′ × 12′ field of 0FGL J1311.9−3419 with 2FGL 95% confidence error ellipse plotted (cyan). The image was binned by 2 × 2 pixels (0.″492 pixel$^{-1}$) and Gaussian smoothed with a kernel radius of 3 pixels. X-ray sources lying within this FOV are marked with their corresponding catalog numbers and are divided into sources outside (white) and inside (yellow: detections; red: tentative sources) the 2FGL ellipse.

(A color version of this figure is available in the online journal.)

the *Chandra* detected sources within the 2FGL 95% confidence error ellipses. As the LAT localization errors for the two targets are different, we set separate detection thresholds, $P_B < 5.4 \times 10^{-6}$ for 0FGL J1311.9−3419 and $<1.8 \times 10^{-6}$ for 0FGL J1653.4−0200, in any of the three defined X-ray energy bands. This corresponds to less than one false positive source due to background fluctuations within each 2FGL ellipse. For 0FGL J1311.9−3419 and 0FGL J1653.4−0200, we detected nine and 13 such X-ray sources, while an additional two and seven tentative ones (those that did not pass the detection threshold) were found, respectively. In Table 2, we provide selected information for these X-ray sources taken from Appendix A. It is apparent from the table that our choices for the probability thresholds divided detected X-ray sources into ones with $\gtrsim$4 net counts and $>1.0\sigma$ in the full (0.5–8 keV) band, while those with ∼3 net counts and $\lesssim 1.0\sigma$ were deemed tentative. The detected sources are indicated by yellow markers in Figures 1 and 2, while the tentative ones are indicated by red markers (the latter are no longer discussed in the main text of the paper). In Table 2, we also provide 0.5–8 keV fluxes. For the brightest sources (CXOU J131145.7−343030 = N35, CXOU J165338.0−015836 = N38, and CXOU J165341.4−015927 = N44), the fluxes are from detailed spectral fits (Section 2.2), while for the remaining fainter sources, we estimated fluxes using exposure corrected count rates and a conversion $10^{-3}$ counts s$^{-1}$ = $10^{-14}$ erg s$^{-1}$ cm$^{-2}$, calculated from PIMMS[11] assuming a single power law with photon index, $\Gamma = 2$.

### 2.2. Further X-Ray Analysis for Selected Sources and Multi-wavelength Counterpart Matches

Several X-ray sources have sufficient statistics to perform more detailed spectral and temporal analysis and these results are presented in the following (Sections 2.2.1 and 2.2.2). Specifically, we studied the brightest X-ray sources within the 2FGL error ellipses, namely, CXOU J131145.7−343030 (Figure 1) and CXOU J165338.0−015836 (Figure 2), with respective 0.5–8 keV count rates of $(2.72 \pm 0.37) \times 10^{-3}$ counts s$^{-1}$ and $(14.78 \pm 0.84) \times 10^{-3}$ counts s$^{-1}$. As mentioned (Section 2), the former count rate is relatively low because the X-ray source fell on a gap between the ACIS-I CCDs. Another X-ray bright source (CXOU J131145.7−343030; $(5.73 \pm 0.54) \times 10^{-3}$ counts s$^{-1}$) just outside and to the south of the 2FGL error ellipse (Figure 1) was previously detected in a *Suzaku* observation (Maeda et al. 2011), so it is also discussed here. Light curves for these sources were generated (Figure 3),

[11] http://cxc.harvard.edu/toolkit/pimms.jsp

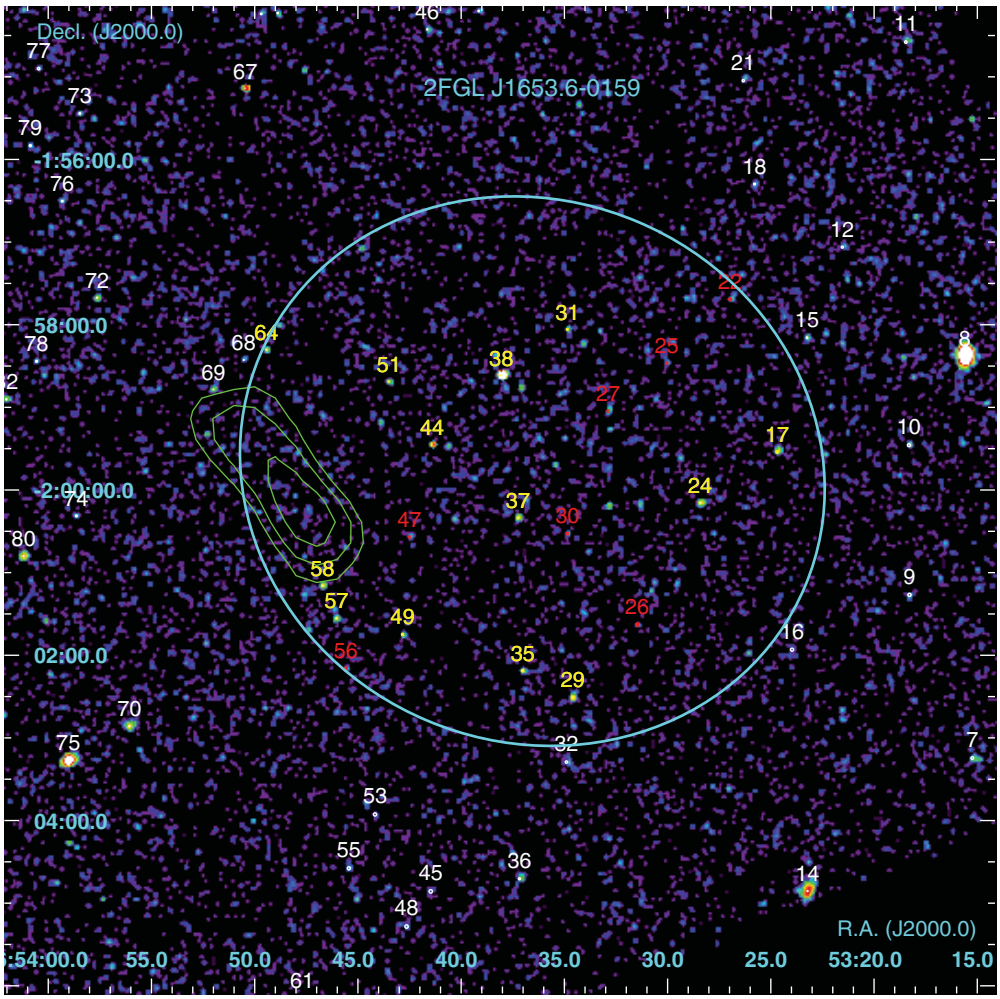


**Figure 2.** Same as in Figure 1, but for 0FGL J1653.4−0200. In addition, the NVSS 1.4 GHz radio contours for NVSS J165348.44−015958.7 (discussed in Section 3) are indicated in green contours (levels of 1.5, 2.1, and 3.0 mJy beam$^{-1}$; 45″ beam).

(A color version of this figure is available in the online journal.)

confirming the finding based on the KS test (Section 2.1) that there is no significant X-ray variability within the ∼20 ks observation span. Their X-ray spectra, along with that of the second brightest X-ray source within the 2FGL error ellipse of 0FGL J1653.4−0200 (CXOU J165341.4−015927) were analyzed using XSPEC v12, considering Galactic absorption ($N_{\rm H,Gal}$) values from Kalberla et al. (2005). These X-ray spectral fitting results are summarized in Tables 3 and 4.

From the KS test applied to all the detected X-ray sources (Section 2.1), only one source with possible variability is detected within a *Fermi*-LAT localization ellipse and notes are provided on this object (CXOU J165337.2−020020 in 0FGL J1653.4−0200). Spectral results are additionally provided for the bright, prominent X-ray source, CXOU J165315.6−015822 (seen toward the right edge of Figure 2), found outside of its corresponding 2FGL localization ellipse. For the remaining sources, the statistics allow us to only broadly characterize the hardness or softness of their X-ray spectra.

The typical subarcsecond localizations provided by our *Chandra* observations (Table 2 and Appendix A) allow us to search confidently for optical, near-infrared, mid-infrared, and radio counterparts to the X-ray sources using the USNO B1.0 (Monet et al. 2003), Two Micron All Sky Survey (2MASS; Skrutskie et al. 2006), *WISE* (Wright et al. 2010) from the preliminary data release (WISEP; Cutri et al. 2012), and NVSS (Condon et al. 1998) catalogs. The results of the USNO B1.0, 2MASS, and WISEP catalog matches for the 97 X-ray sources detected in each of the two ACIS-I fields are presented in Appendix B. Of the X-ray sources within the 2FGL 95% confidence error regions of 0FGL J1311.9−3419 and 0FGL J1653.4−0200, and considering optical/infrared sources within 2″ of the X-ray positions, we found 2/9 and 3/13 of the detected sources with USNO B1.0 counterparts, respectively. Of the *Chandra*/USNO B1.0 matches, there was one case in 0FGL J1311.9−3419 where a WISEP match was also found (but without an 2MASS counterpart), and two cases in 0FGL J1653.4−0200 with 2MASS and WISEP counterparts also. There were single detected X-ray sources within the two 2FGL error ellipses where we found possible matches with a WISEP source, but without counterparts in the USNO B1.0 and 2MASS. Specific notes are provided for the optical/infrared matched *Chandra* sources in the following subsections. None of the X-ray sources in the two ACIS-I fields had radio counterparts in the NVSS catalog (45″ resolution at 1.4 GHz with typical sensitivity level of ∼2.5 mJy) out to a 45″ search radius. In fact, within the 2FGL 95% confidence ellipses of the two $\gamma$-ray objects, only one NVSS source is found (within 0FGL J1653.4−0200; see Figure 2) and it is briefly discussed in Section 3.

**Table 2**
Detected and Tentatively Detected (Catalog Numbers, *N*, Marked with Asterisk) *Chandra* X-Ray Sources within the 2FGL Error Ellipses of 0FGL J1311.9−3419 and 0FGL J1653.4−0200

| *N* | CXOU Name | *r* (″) | Counts (0.5–8 keV) | $\sigma$ | Counts (0.5–2 keV) | Counts (2–8 keV) | $F_{0.5-8\,\mathrm{keV}}$ |
|---|---|---|---|---|---|---|---|
| | | | 0FGL J1311.9−3419 | | | | |
| 26 | J131139.3−342829 | 0.23 | 5.9 (+3.6/−2.4) | 1.6 | 4.0 (+3.2/−1.9) | 1.9 (+2.7/−1.3) | 0.3 |
| 27 | J131140.0−343023 | 0.30 | 3.9 (+3.2/−1.9) | 1.2 | 2.0 (+2.7/−1.3) | 1.9 (+2.7/−1.3) | 0.2 |
| 29 | J131141.9−342955 | 0.19 | 6.9 (+3.8/−2.6) | 1.8 | 1.0 (+2.3/−0.8) | 6.0 (+3.6/−2.4) | 0.4 |
| 31 | J131143.7−342749 | 0.26 | 3.9 (+3.2/−1.9) | 1.2 | 3.0 (+2.9/−1.6) | 0.9 (+2.3/−0.8) | 0.2 |
| 33 | J131144.6−343100 | 0.24 | 4.9 (+3.4/−2.2) | 1.4 | 2.0 (+2.7/−1.3) | 3.0 (+2.9/−1.6) | 0.3 |
| 35 | J131145.7−343030 | 0.07 | 54.0 (+8.4/−7.3) | 6.4 | 32.0 (+6.7/−5.6) | 22.0 (+5.8/−4.7) | 10.3 |
| 38 | J131146.4−343050 | 0.18 | 7.9 (+4.0/−2.8) | 2.0 | 2.0 (+2.7/−1.3) | 6.0 (+3.6/−2.4) | 0.4 |
| 40 | J131147.0−342953 | 0.21 | 4.0 (+3.2/−1.9) | 1.2 | 3.0 (+2.9/−1.6) | 1.0 (+2.3/−0.8) | 0.2 |
| 47 | J131150.5−343029 | 0.23 | 3.9 (+3.2/−1.9) | 1.2 | 3.0 (+2.9/−1.6) | 1.0 (+2.3/−0.8) | 0.2 |
| 30* | J131143.3−342826 | 0.27 | 2.9 (+2.9/−1.6) | 1.0 | −0.0 (+1.9/−0.0) | 3.0 (+2.9/−1.6) | 0.2 |
| 42* | J131149.0−342829 | 0.23 | 3.0 (+2.9/−1.6) | 1.0 | 1.0 (+2.3/−0.8) | 2.0 (+2.7/−1.3) | 0.2 |
| | | | 0FGL J1653.4−0200 | | | | |
| 17 | J165324.6−015932 | 0.40 | 10.5 (+4.4/−3.3) | 2.4 | 6.8 (+3.8/−2.6) | 3.7 (+3.2/−1.9) | 0.7 |
| 24 | J165328.4−020009 | 0.28 | 13.7 (+4.8/−3.7) | 2.8 | 11.9 (+4.6/−3.4) | 1.8 (+2.7/−1.3) | 0.8 |
| 29 | J165334.5−020230 | 0.38 | 13.5 (+4.8/−3.7) | 2.8 | 7.8 (+4.0/−2.8) | 5.7 (+3.6/−2.4) | 0.7 |
| 31 | J165334.8−015803 | 0.23 | 4.9 (+3.4/−2.2) | 1.4 | 3.0 (+2.9/−1.6) | 2.0 (+2.7/−1.3) | 0.3 |
| 35 | J165337.0−020211 | 0.49 | 5.6 (+3.6/−2.4) | 1.6 | 4.8 (+3.4/−2.2) | 0.8 (+2.3/−0.8) | 0.3 |
| 37 | J165337.2−020020 | 0.18 | 11.9 (+4.6/−3.4) | 2.6 | 5.0 (+3.4/−2.2) | 6.9 (+3.8/−2.6) | 0.6 |
| 38 | J165338.0−015836 | 0.03 | 306.9 (+18.5/−17.5) | 16.6 | 198.0 (+15.1/−14.1) | 109.0 (+11.5/−10.4) | 23.1 |
| 44 | J165341.4−015927 | 0.10 | 18.9 (+5.4/−4.3) | 3.5 | 17.0 (+5.2/−4.1) | 2.0 (+2.7/−1.3) | 0.7 |
| 49 | J165342.8−020144 | 0.38 | 5.8 (+3.6/−2.4) | 1.6 | 5.9 (+3.6/−2.4) | −0.1 (+1.9/−0.0) | 0.3 |
| 51 | J165343.4−015841 | 0.16 | 5.9 (+3.6/−2.4) | 1.6 | 6.0 (+3.6/−2.4) | −0.0 (+1.9/−0.0) | 0.3 |
| 57 | J165346.0−020133 | 0.28 | 8.8 (+4.1/−2.9) | 2.1 | 6.9 (+3.8/−2.6) | 1.9 (+2.7/−1.3) | 0.5 |
| 58 | J165346.7−020109 | 0.21 | 11.8 (+4.6/−3.4) | 2.6 | 5.9 (+3.6/−2.4) | 5.9 (+3.6/−2.4) | 0.6 |
| 64 | J165349.4−015818 | 0.20 | 6.0 (+3.6/−2.4) | 1.7 | 1.0 (+2.3/−0.8) | 5.0 (+3.4/−2.2) | 0.5 |
| 22* | J165326.9−015741 | 0.61 | 2.7 (+2.9/−1.6) | 0.9 | 1.9 (+2.7/−1.3) | 0.8 (+2.3/−0.8) | 0.2 |
| 25* | J165330.0−015827 | 0.45 | 2.8 (+2.9/−1.6) | 1.0 | 1.9 (+2.7/−1.3) | 0.9 (+2.3/−0.8) | 0.2 |
| 26* | J165331.4−020137 | 0.73 | 2.6 (+2.9/−1.6) | 0.9 | −0.2 (+1.9/−0.0) | 2.8 (+2.9/−1.6) | 0.1 |
| 27* | J165332.8−015902 | 0.37 | 2.9 (+2.9/−1.6) | 1.0 | 0.9 (+2.3/−0.8) | 1.9 (+2.7/−1.3) | 0.2 |
| 30* | J165334.8−020031 | 0.43 | 2.9 (+2.9/−1.6) | 1.0 | −0.1 (+1.9/−0.0) | 2.9 (+2.9/−1.6) | 0.2 |
| 47* | J165342.4−020034 | 0.36 | 3.0 (+2.9/−1.6) | 1.0 | 2.0 (+2.7/−1.3) | 1.0 (+2.3/−0.8) | 0.3 |
| 56* | J165345.5−020209 | 0.63 | 2.7 (+2.9/−1.6) | 0.9 | 0.8 (+2.3/−0.8) | 1.8 (+2.7/−1.3) | 0.1 |

**Notes.** Listed are the J2000.0 coordinate based names, error radius (*r*), net counts in each of the three defined energy bands, and significance ($\sigma$) in the 0.5–8 keV band. The 0.5–8 keV fluxes ($F_{0.5-8\,\mathrm{keV}}$; in units of $10^{-14}$ erg s$^{-1}$ cm$^{-2}$) are from the spectral fits for the brightest sources (Tables 3 and 4), while the estimates for the remaining fainter sources are described in Section 2.1.

#### 2.2.1. 0FGL J1311.9−3419 Field

*CXOU J131143.7−342749 (N31).* We found that this X-ray source is the only other source (the other case being CXOU J131145.7−343030 below) within the 0FGL J1311.9−3419 2FGL ellipse with an optical counterpart. With only ∼4 net counts detected in the 0.5–8 keV band (1.2$\sigma$), its spectrum is undersampled. The X-ray centroid, however, is well determined ($r = 0\farcs26$, statistical) and is offset by only $0\farcs37$ from an optical source (USNO B1.0 0555−0290806; $B2 = 19.67$, $R2 = 18.87$, $I = 18.33$ mag) that has a mid-IR counterpart (WISEP J131143.72−342749.9; $W1 = 15.790$, $W2 = 15.302$, $W3 = 11.432$, $W4 = 7.954$ mag), but no near-IR counterpart in the 2MASS.

*CXOU J131145.7−343030 (N35).* This is the brightest X-ray source within the 2FGL error ellipse of 0FGL J1311.9−3419. Its X-ray spectrum (Figure 4, left) is best fit with an absorbed single power law with $\Gamma = 1.3 \pm 0.4$ ($N_{\mathrm{H,Gal}} = 4.95 \times 10^{20}$ cm$^{-2}$), and an observed 0.5–8 keV flux of $(9.9^{+2.9}_{-2.7}) \times 10^{-14}$ erg s$^{-1}$ cm$^{-2}$. Due to the low statistics and the already low $N_{\mathrm{H,Gal}}$ value, we found that the spectrum could also be fit without an absorption component, with $\Gamma = 1.1 \pm 0.4$. We quote the model parameters with the absorption included (Table 3) to compare to the *Suzaku* results from Maeda et al. (2011), who detected this source (named "src A" therein) on 2009 August 4, seven months prior to our *Chandra* observation. The *Suzaku* data revealed short-term variability in the form of a factor ∼10 X-ray flare in the first 20 ks of the 100 ks duration observation (33 ks net exposure). The *Suzaku* measured photon index ($\Gamma = 1.38 \pm 0.13$) is consistent with that measured in our *Chandra* observation, but the overall average 2–8 keV flux of $(14.5 \pm 1.8) \times 10^{-14}$ erg s$^{-1}$ cm$^{-2}$ is ∼2× larger. With the improved *Chandra* point-spread function over the *Suzaku* one, we detect several additional fainter X-ray sources near this bright source (e.g., N38 and N33; Figure 1), but due to their low count rates, they cannot be wholly responsible for the higher measured flux in the *Suzaku* observation. CXOU J131145.7−343030 was also detected toward the edge of the FOV of a *Swift* (Gehrels et al. 2004) observation (3.34 ks, ObsID 31358) from 2009 February 27 with the X-ray telescope (XRT; Burrows et al. 2005). The 0.3–10 keV XRT count rate of $(4.5 \pm 1.4) \times 10^{-3}$ counts s$^{-1}$ is equivalent to a 0.5–8 keV flux of $\sim 2 \times 10^{-13}$ erg s$^{-1}$ cm$^{-2}$, indicating a

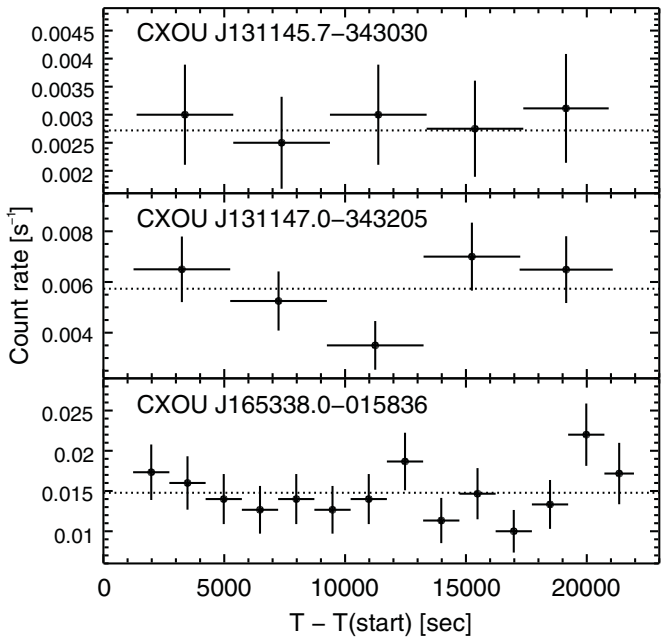


**Figure 3.** *Chandra* ACIS-I (0.5–8 keV) light curves of the brightest X-ray source within (CXOU J131145.7−343030, top) and just outside and to the south (CXOU J131147.0−343205, middle) of the 2FGL error ellipse of 0FGL J1311.9−3419, and the brightest X-ray source within the 2FGL error ellipses of 0FGL J1653.4−0200 (CXOU J165338.0−015836, bottom). The data points are shown in time bins that are 4 ks (∼10 counts per bin), 4 ks (∼20 counts per bin), and 1.5 ks (∼20 counts per bin) long, respectively. The times are indicated relative to the observation start times (Table 1) and the average count rates are indicated with horizontal dotted lines.

∼2× brighter source about one year prior to the *Chandra* observation, providing further evidence that the X-ray source faded since 2009. We found that this bright *Chandra* source has an optical counterpart (USNO B1.0 0554−0289419, 0.″62 offset) with $B2 = 21.02$ mag.

*CXOU J131147.0−343205 (N39).* Although this relatively bright X-ray source is outside (to the south) of the 2FGL error ellipse, we provide notes on it because it was the only other X-ray source detected in the *Suzaku* observation mentioned above (Maeda et al. 2011, "src B" therein). For an absorbed single power-law fit to the *Chandra* X-ray spectrum (Figure 4, right), we required an absorption component with a value, $N_{\rm H} = (45^{+36}_{-29}) \times 10^{20}$ cm$^{-2}$, well above the Galactic one. The *Chandra* observed photon index and 2–8 keV flux (Table 3) are consistent with the *Suzaku* measured values of $\Gamma = 1.34^{+0.16}_{-0.15}$ and $(12.0^{+1.8}_{-1.7}) \times 10^{-14}$ erg s$^{-1}$ cm$^{-2}$, indicating a relatively stable X-ray flux on months' timescale. This source was outside the FOV of the *Swift* XRT observation discussed above (ObsID 31358). With the improved *Chandra* localization, we found a mid-infrared counterpart (WISEP J131147.09−343205.3; $W1 = 15.720$, $W2 = 14.949$, $W3 = 12.226$, $W4 = 9.056$ mag), but no corresponding source in the USNO B1.0 or 2MASS catalogs. Other than being relatively bright in X-rays, its location outside of the 2FGL error ellipse does not make it a particularly likely counterpart to the $\gamma$-ray source.

*CXOU J131147.0−342953 (N40).* This faint X-ray source is the closest one detected to the 2FGL centroid (Figure 1). It has a possible mid-IR counterpart (WISEP J131147.15−342953.5; $W1 = 16.846$, $W2 = 16.408$, $W3 = 12.443$, $W4 = 8.721$ mag) offset by 1.″25 from the *Chandra* position. We found no optical and near-IR counterparts to this source to the limit of the USNO B1.0 and 2MASS catalogs, respectively.

**Table 3**
*Chandra* Spectral Parameters for the Brightest X-Ray Source within (CXOU J131145.7−343030) and Just Outside and to the South of (CXOU J131147.0−343205) the 2FGL Error Ellipse of 0FGL J1311.9−3419

| Parameter | CXOU J131145.7−343030 Value and Error | CXOU J131147.0−343205 Value and Error |
|---|---|---|
| $N_{\rm H,Gal}$ ($10^{20}$ cm$^{-2}$) | 4.95 (fixed) | 4.95 (fixed) |
| $N_{\rm H}$ ($10^{20}$ cm$^{-2}$) | ... | $45^{+36}_{-29}$ |
| $\Gamma$ | $1.3 \pm 0.4$ | $1.6 \pm 0.5$ |
| $c$-stat/dof | 201/510 | 297/509 |
| $F_{0.5-8\,\rm keV}$: obs, unabs | $9.9^{+2.9}_{-2.7}$, 10.3 | $10.7^{+1.5}_{-3.1}$, 14.5 |
| $F_{0.5-2\,\rm keV}$: obs, unabs | $2.4^{+0.6}_{-0.8}$, 2.7 | $2.0^{+0.4}_{-0.8}$, 5.3 |
| $F_{2-8\,\rm keV}$: obs, unabs | $7.5^{+3.0}_{-2.3}$, 7.6 | $8.7^{+2.2}_{-3.0}$, 9.1 |

**Notes.** These are the *Suzaku* detected sources, named src A and src B, respectively, by Maeda et al. (2011). Fluxes ($F$) as observed (obs) and unabsorbed (unabs) are in units of $10^{-14}$ erg s$^{-1}$ cm$^{-2}$. Errors quoted are at 90% confidence.

**Table 4**
As in Table 3, but for the Brightest (CXOU J165338.0−015836) and Second Brightest (CXOU J165341.4−015927) X-Ray Sources within the 2FGL Error Ellipse of 0FGL J1653.4−0200

| Parameter | CXOU J165338.0−015836 Value and Error | CXOU J165341.4−015927 Value and Error |
|---|---|---|
| $N_{\rm H,Gal}$ ($10^{20}$ cm$^{-2}$) | 8.18 (fixed) | ... |
| $N_{\rm H}$ ($10^{20}$ cm$^{-2}$) | $9^{+13}_{-9}$ | $0^{+27}_{-0}$ |
| $\Gamma$ | $1.8 \pm 0.3$ | ... |
| $kT$ (keV) | ... | $0.4^{+0.2}_{-0.1}$ |
| $c$-stat/dof | 335/509 | 80/235 |
| $F_{0.5-8\,\rm keV}$: obs, unabs | $19.3^{+2.1}_{-2.5}$, 23.1 | $0.7^{+0.2}_{-0.3}$, ... |
| $F_{0.5-2\,\rm keV}$: obs, unabs | $6.0^{+0.8}_{-1.2}$, 9.5 | $0.5^{+0.1}_{-0.2}$, ... |
| $F_{2-8\,\rm keV}$: obs, unabs | $13.3^{+2.3}_{-2.2}$, 13.6 | $0.2^{+0.2}_{-0.2}$, ... |

The remaining detected X-ray sources within the 2FGL error ellipse have a range of ∼4–8 net counts (0.5–8 keV), insufficient for detailed spectral or temporal analysis. None have optical/IR counterparts found within 2″ of the *Chandra* positions. Of these, it is worth noting that the two most significant sources appear to have the hardest X-ray spectra, with the ratio of 2–8 keV/0.5–8 keV counts, ∼6/7 (CXOU J131141.9−342955, N29) and ∼6/8 (CXOU J131146.4−343050, N38).

### 2.2.2. 0FGL J1653.4−0200 Field

*CXOU J165315.6−015822 (N8).* This is the brightest X-ray source detected in the ACIS-I field of 0FGL J1653.4−0200, but is 5.′4 offset from the 2FGL centroid and outside of the 95% confidence error ellipse ($r \simeq 3.'6$; see Figure 2). It was probably detected previously as the faint RASS source 1RXS J165312.9−015819 (Voges et al. 2000), being only 41″ away. The *Chandra* position is coincident (0.″50 offset) with the optical source USNO B1.0 0880−0368721 ($B2 = 18.47$, $R2 = 16.97$, $I = 16.96$ mag), which is also detected in the near-IR (2MASS J16531562−0158224; $J = 16.196$, $H = 15.560$, $K = 14.292$ mag) and mid-IR (WISEP J165315.62−015822.3; $W1 = 12.599$, $W2 = 11.578$, $W3 = 9.208$, $W4 = 7.364$ mag). Its X-ray spectrum (not shown) is well fit ($c$-stat/dof = 427/510) with an absorbed power law with $\Gamma = 1.86 \pm 0.08$ ($N_{\rm H,Gal} = 8.18 \times 10^{20}$ cm$^{-2}$ fixed), and an observed 0.5–8 keV flux $(14.1 \pm 0.6) \times 10^{-13}$ erg s$^{-1}$ cm$^{-2}$ ($15.7 \times 10^{-13}$ erg s$^{-1}$ cm$^{-2}$, unabsorbed). Leaving the absorption

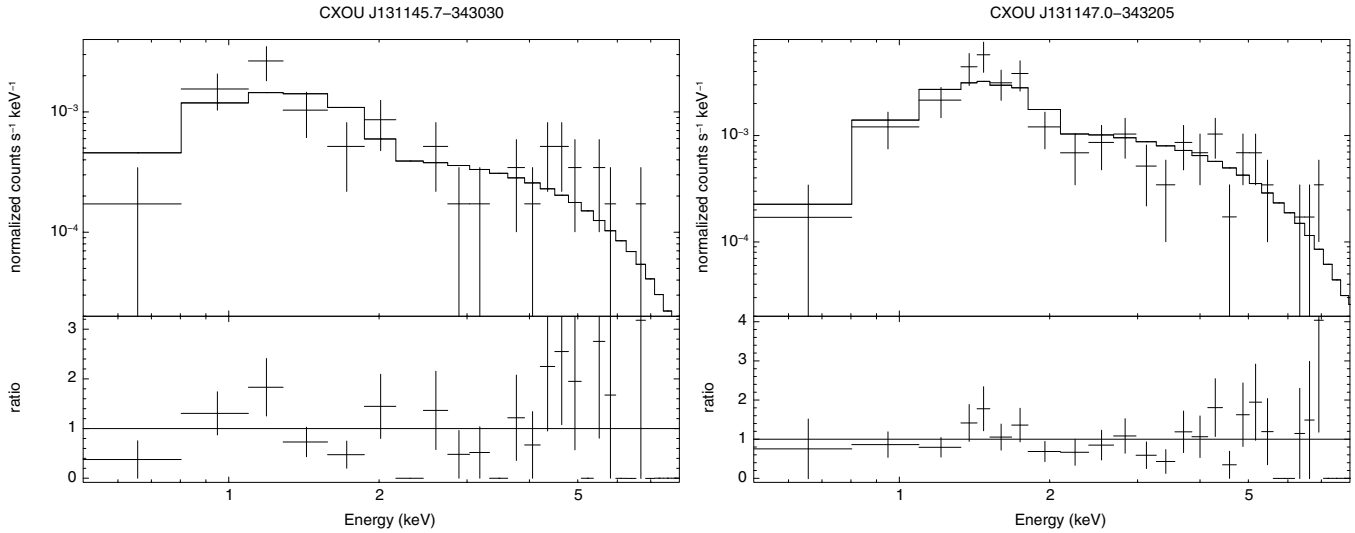


**Figure 4.** *Chandra* ACIS-I spectrum of the brightest X-ray source within the 2FGL error ellipse of 0FGL J1311.9−3419 (CXOU J131145.7−343030, N35; left), and of the bright X-ray source just outside (to the south of) the error ellipse (CXOU J131147.0−343205, N39; right). The top panels show the data points with the line indicating the best-fit absorbed single power-law models and the bottom panels show the ratio between the data and the models.

as a free parameter, we found negligible change in the photon index ($1.83 \pm 0.13$), and the derived $N_{\rm H} = (7 \pm 5) \times 10^{20}$ cm$^{-2}$ converges toward the Galactic value. The absence of a radio counterpart in the NVSS (∼2.5 mJy limit at 1.4 GHz) makes it unlikely to be a $\gamma$-ray-emitting AGN. Although this source is quite prominent in X-rays, its placement outside the 2FGL 95% confidence ellipse means it is probably unrelated to 0FGL J1653.4−0200.

*CXOU J165337.2−020020 (N37).* This faint X-ray source near the measured 2FGL centroid is the only one within the LAT localizations of either source studied that is possibly variable ($P_{\rm K-S} = 0.012$; Section 2.1). Note however that this result is based on only ∼12 net counts detected. There is no optical counterpart to the ∼21 mag limit of the USNO B1.0 catalog, nor was there a positional match in the 2MASS and WISEP catalogs.

*CXOU J165338.0−015836 (N38).* This is the brightest X-ray source found within the 2FGL error ellipse of 0FGL J1653.4−0200. To its X-ray spectrum (Figure 5, left), we fitted an absorbed single power law with $\Gamma = 1.8 \pm 0.3$, and found a hint of an additional absorption component with $N_{\rm H} = (9^{+13}_{-9}) \times 10^{20}$ cm$^{-2}$ larger than the Galactic value ($N_{\rm H,Gal} = 8.18 \times 10^{20}$ cm$^{-2}$). We found that a pure power-law model without any absorption overestimates the soft part of the spectrum, and thus was a poor model for the data. This X-ray source was also detected in a snapshot *Swift* XRT observation (4.85 ks, ObsID 31379) from 2009 March 22 with a 0.3–10 keV count rate of $(3.2 \pm 1.1) \times 10^{-3}$ counts s$^{-1}$. This is equivalent to a 0.5–8 keV flux of $\sim 16 \times 10^{-14}$ erg s$^{-1}$ cm$^{-2}$, indicating a roughly stable flux relative to the *Chandra* observed value, $(19.3^{+2.1}_{-2.5}) \times 10^{-14}$ erg s$^{-1}$ cm$^{-2}$ (Table 4) obtained ∼10 months later. This X-ray source has an optical counterpart, USNO B1.0 0880−0369025 ($B2 = 20.40$, $R2 = 19.41$, and $I = 20.0$ mag), which is only 0.″28 offset from the *Chandra* determined centroid.

*CXOU J165341.4−015927 (N44).* This is the second brightest X-ray source found within the 2FGL error ellipse of 0FGL J1653.4−0200. Only ∼19 net counts (0.5–8 keV) were found, with most of the counts (17) in the 0.5–2 keV range indicating a soft X-ray spectrum. Despite the low statistics, the X-ray spectrum can be fit with a blackbody model (Figure 5, right), with temperature, $kT = 0.4^{+0.2}_{-0.1}$ keV, and absorption consistent with zero (Table 4). We found an optical source, USNO B1.0 0880−0369077 ($B2 = 20.58$, $R2 = 18.95$, and $I = 17.05$ mag) 0.″68 offset from the X-ray centroid. The USNO source has a near-infrared (2MASS J16534140−0159272; $J = 15.094$, $H = 14.469$, $K = 14.147$ mag) and a mid-infrared (WISEP J165341.41−015927.6; $W1 = 14.057$, $W2 = 13.843$, $W3 = 12.569$, $W4 = 8.667$ mag) counterpart.

*CXOU J165342.8−020144 (N49).* This is the only other X-ray source within the 2FGL ellipse of 0FGL J1653.4−0200 (other than the two mentioned sources above, N38 and 44) with a USNO B1.0 catalog match. The X-ray source is offset by 0.″32 from the relatively bright optical source ($B2 = 16.64$, $R2 = 14.60$, $I = 14.16$ mag), USNO B1.0 0879−0416658. The USNO source has a near-infrared (2MASS J16534285−0201450; $J = 13.133$, $H = 12.575$, $K = 12.492$ mag) and mid-infrared (WISEP J165342.83−020145.1; $W1 = 12.420$, $W2 = 12.429$, $W3 = 12.292$, $W4 = 9.014$ mag) counterpart. Although the source is faint ($1.6\sigma$ in the 0.5–8 keV band), all six of its detected counts are in the 0.5–2 keV range indicating a soft spectrum.

*CXOU J165343.4−015841 (N51).* The X-ray spectrum of this faint source appears soft with all of its ∼6 detected net counts in the 0.5–2 keV band. It is the only case of a detected X-ray source within the 2FGL ellipse of 0FGL J1653.4−0200 that has a mid-IR counterpart (0.″7 offset from WISEP J165343.52−015840.6; $W1 = 16.245$, $W2 = 16.366$, $W3 = 12.612$, $W4 = 8.882$ mag) and without a match in the USNO B1.0 and 2MASS catalogs.

Among the remaining detected X-ray sources within the 2FGL error ellipse, only ∼5–14 net counts (0.5–8 keV) are observed per object. Although the statistics are limited, we found that several sources have most of their detected counts in either the 0.5–2 keV or 2–8 keV range, indicating soft and hard spectra, respectively. As was the case for the two faint sources noted above (CXOU J165342.8−020144 = N49 and CXOU J165343.4−015841 = N51), we found that CXOU J165328.4−020009 (N24) has an indication for a soft spectrum, with a ratio of 0.5–2 keV/0.5–8 keV counts, ∼12/14. Similarly, the hardest spectrum source has a ratio of 2–8 keV/0.5–8 keV counts, ∼5/6 (CXOU J165349.4−015818 = N64).

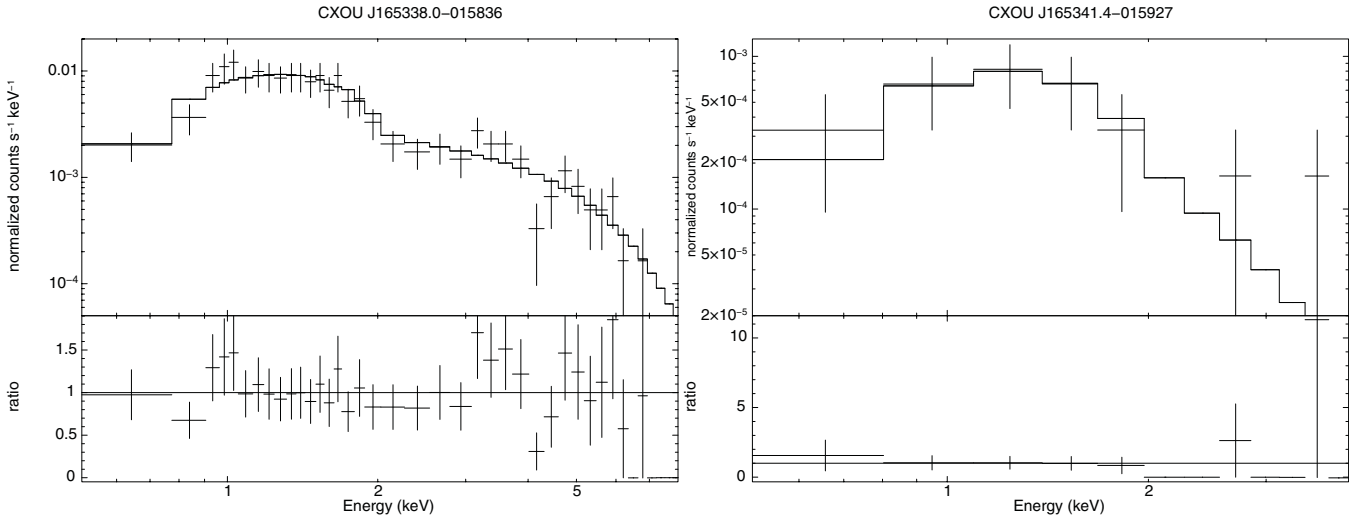


**Figure 5.** *Chandra* ACIS-I spectrum of the brightest (CXOU J165338.0−015836, N38; left) and the second brightest (CXOU J165341.4−015927, N44; right) X-ray sources within the 2FGL error ellipse of 0FGL J1653.4−0200. The top panels show the data points with the line indicating the best-fit absorbed single power-law and blackbody models, respectively, and the bottom panels show the ratio between the data and the models.

The latter two sources do not have optical/IR counterparts at the sensitivity limits of the USNO B1.0, 2MASS, and WISEP catalogs.

## 3. DISCUSSION

The $\gamma$-ray sources studied, 0FGL J1311.9−3419 and 0FGL J1653.4−0200, are the two brightest unidentified *Fermi*-LAT sources found at high Galactic latitudes. In fact, both have been detected by EGRET (Section 1), and the improved localizations provided now by the *Fermi*-LAT with $r_{95} \simeq 2\farcm0$–$3\farcm6$ (compared with the corresponding EGRET values $\simeq 34'$–$44'$; Hartman et al. 1999) allow us to address the counterparts with more certainty. From an X-ray perspective, our *Chandra* observations detected sources down to a 0.5–8 keV flux threshold of $\sim(0.2\text{–}0.3) \times 10^{-14}$ erg s$^{-1}$ cm$^{-2}$ (Table 2). This is much improved over typical flux limits of $\sim 10^{-13}$ erg s$^{-1}$ cm$^{-2}$ achieved in all-sky surveys like the RASS (0.1–2.4 keV; Voges et al. 1999, 2000). Also, existing pointed *Swift* and *Suzaku* observations (Section 2.2) detected only the single brightest source within the LAT error ellipses, compared with the 9 and 13 *Chandra* detected X-ray sources that can now be considered as potential counterparts to the LAT $\gamma$-ray source.

Due to their high Galactic latitudes, the most obvious candidate counterparts to these unidentified $\gamma$-ray sources would be extragalactic objects, specifically, blazars fainter than currently cataloged. The LAT error circles of the high latitude objects have in fact been searched for blazars down to a radio flux limit of $\sim$30 mJy (Abdo et al. 2009b), but even fainter blazars are now being found in large numbers, e.g., from cross-correlations of the SDSS/RASS/FIRST databases (e.g., Plotkin et al. 2008). In this context however, we found that none of the detected X-ray sources in either field had radio counterparts in the NVSS catalog (Section 2.2). In fact, only one (extended) radio source was found within the 95% LAT error ellipse of 0FGL J1653.4−0200 (below), with none detected within the 0FGL J1311.9−3419 localization. The NVSS flux limit of $\sim$2.5 mJy at 1.4 GHz is $\sim 10\times$ fainter than the faintest typical radio sources currently associated with *Fermi*-LAT $\gamma$-ray blazars (Ackermann et al. 2011a, 2011b). This absence of radio sources in general, and the lack of point source counterparts to the X-ray detected objects specifically, allows us to rule out faint blazars as possible counterparts of these sources. Radio-quiet AGNs are not currently known to be $\gamma$-ray emitters, except for a few examples of nearby galaxies with substantial starburst contributions (Ackermann et al. 2011a, 2012; Lenain et al. 2010; Teng et al. 2011), so even if the *Chandra* detected X-ray sources are confirmed to be AGN, they are likely unrelated to the $\gamma$-ray source.

From a $\gamma$-ray perspective, the faintest radio blazars tend to have harder HE $\gamma$-ray spectra ($\Gamma < 2$), sometimes extending into TeV energies. Unlike these blazars, the two $\gamma$-ray sources discussed are characterized by soft 0.1–100 GeV spectra, being parameterized with single power laws in the 1FGL catalog analysis (Abdo et al. 2010a) with slopes, $\Gamma = 2.25 \pm 0.05$ (0FGL J1311.9−3419) and $2.29 \pm 0.06$ (0FGL J1653.4−0200). In fact, a more detailed analysis of the longer two-year LAT data set presented in the 2FGL catalog indicated the HE spectra were best characterized as log-parabolas (Nolan et al. 2012),[12] not typically observed in $\gamma$-ray blazars (Abdo et al. 2010d). Moreover, unlike typical bright $\gamma$-ray-emitting blazars, their variability indices of 17–19 are below the 41.6 threshold in the 2FGL catalog analysis (Nolan et al. 2012), indicating no significant $\gamma$-ray variability within the 24 month data set.[13]

Nearby radio galaxies have been found to be likely $\gamma$-ray emitters (e.g., Ackermann et al. 2011a, and references therein) and it is possible that some fraction of the unidentified high Galactic latitude LAT sources could be unknown radio galaxies (i.e., "misaligned blazars") that could be faint X-ray emitters (e.g., Canosa et al. 1999). In particular, steady $\gamma$-ray emission from radio lobes is possible (Cheung 2007), as was observed in the nearby radio galaxy Centaurus A (Abdo et al. 2010e) and possibly in NGC 6251 (Takeuchi et al. 2012). In this context, the single radio source (NVSS J165348.44−015958.7; $11.5 \pm 1.7$ mJy at 1.4 GHz) found within the 0FGL J1653.4−0200 error ellipse is extended, with measured elliptical dimensions, major axis $= 125\farcs4$, minor axis $< 46\farcs9$ (i.e., unresolved in this direction), at position angle $= 36^\circ$. Inspecting Figure 2, we see

[12] http://heasarc.gsfc.nasa.gov/FTP/fermi/data/lat/catalogs/source/lightcurves/2FGL_J1311d7m3429_spec.png, http://heasarc.gsfc.nasa.gov/FTP/fermi/data/lat/catalogs/source/lightcurves/2FGL_J1653d6m0159_spec.png

[13] http://heasarc.gsfc.nasa.gov/FTP/fermi/data/lat/catalogs/source/lightcurves/2FGL_J1311d7m3429_lc.png, http://heasarc.gsfc.nasa.gov/FTP/fermi/data/lat/catalogs/source/lightcurves/2FGL_J1653d6m0159_lc.png

that the *Chandra* sources N58 and N57 (within the 2FGL ellipse) and N69 (outside the 2FGL ellipse) are located near the extended tips of this radio source. If any of these *Chandra* sources are related to NVSS J165348.44−015958.7, it could plausibly mark a radio outflow from the X-ray source. However, the lack of an optically bright extended giant elliptical galaxy counterpart to any of these X-ray sources eliminates the possibility that these are nearby radio galaxies. Relatedly, young radio sources are expected to be steady $\gamma$-ray emitters (e.g., McConville et al. 2011), but such objects are typically bright compact centimeter-wavelength sources and no such sources were found in the NVSS image within the LAT error regions in the present cases.

As AGNs likely can be ruled out as potential counterparts, the remaining possibilities are open to debate. As both $\gamma$-ray sources are located at mid Galactic latitudes ($|b| = 10°$–$30°$; Table 1), there is the interesting possibility of isolated neutron stars associated with the $\gamma$-ray sources, as was posited for 3EG J1835+5918 (Halpern et al. 2002, and references therein), and subsequently confirmed with *Fermi*-LAT observations of this (Abdo et al. 2010b) and other pulsars (Abdo et al. 2010c). Indeed, 0FGL J1311.9−3419 and 0FGL J1653.4−0200 are two of nine total high Galactic latitude ($|b| > 10°$) $\gamma$-ray sources from the LAT bright source list (Abdo et al. 2009a) that were unidentified at the time. The other seven sources have all since been identified as pulsar powered sources. Specifically, they were predominantly identified as radio/$\gamma$-ray-emitting MSPs—PSR J0614−3329, PSR J1231−1411, PSR J2214+3000 (Ransom et al. 2011), PSR J2241−5236 (Keith et al. 2011), and PSR J2302+4442 (Cognard et al. 2011)—with one normal young pulsar (PSR J2055+25; Saz Parkinson et al. 2010). The two subjects of the present study have been similarly searched for pulsating radio emission with null results in the past (based on their EGRET localizations; Crawford et al. 2006) and in new searches of the *Fermi* error circles (Ransom et al. 2011). In the remaining case (0FGL J2339.8−0530), the brightest *Chandra* X-ray source within the *Fermi*-LAT error ellipse was found to be a black widow-type MSP and is the likely counterpart of the $\gamma$-ray source (Kong et al. 2012; see also Romani & Shaw 2011). As in these other seven 0FGL cases, the LAT spectra of our remaining two unidentified objects display significant curvature[12] and are steady $\gamma$-ray emitters,[13] so may point to a pulsar origin for them as well.

In our *Chandra* observations of the MSPs identified with the LAT sources, PSR J2214+3000 (Ransom et al. 2011) and PSR J2241−5236 (Keith et al. 2011), the MSPs were spatially coincident with the brightest X-ray sources within the LAT error ellipses. The X-ray spectral analysis indicated a thermal origin with best-fit blackbody temperatures, $kT \sim 0.2$–$0.3$ keV, with essentially no photons above 2 keV. Similar X-ray spectral results for the other identified pulsars were derived from *XMM* observations of PSR J2302+4442 (Cognard et al. 2011) and *Swift* observations of PSR J0614−3329 and PSR J1231−1411 (Ransom et al. 2011); see also past *XMM* observations of the 0FGL J0614.3−3330 case (La Palombara et al. 2006). In fact, we found that several X-ray sources (Section 2.2) have soft spectra that appear thermal in origin. Taking the 2FGL (Nolan et al. 2012) observed 0.1–100 GeV $\gamma$-ray fluxes for 0FGL J1311.9−3419 ($F_\gamma = 6.17 \times 10^{-11}$ erg s$^{-1}$ cm$^{-2}$) and 0FGL J1653.4−0200 ($F_\gamma = 3.43 \times 10^{-11}$ erg s$^{-1}$ cm$^{-2}$), the *Chandra* observations probe a range of X-ray[14] to $\gamma$-ray flux (or luminosity) ratios, $F_X/F_\gamma \lesssim (2\text{–}8) \times 10^{-3}$ corresponding to the brightest X-ray sources, and down to $\sim(0.04\text{–}0.1) \times 10^{-3}$ for the faintest ones. For a pulsar interpretation, this probes the conversion ranges of spin-down powers to (nonthermal or thermal) X-rays for possible neutron star candidates (e.g., Mirabal et al. 2000).

In contrast to the thermal X-ray sources discussed above, the brightest *Chandra* sources in our two cases show X-ray spectra that extend to ∼7–8 keV and were best fit with single power-law spectra (Section 2.2). If these are the counterparts to the LAT sources, the objects are likely not normal pulsars or MSPs. The nonthermal X-ray spectra of these sources are similar to the case of CXOU J233938.7−053305, the putative counterpart of the (formerly) unidentified high Galactic latitude source 0FGL J2339.8−0530 (Kong et al. 2012). In the latter case, the spectrum is best characterized by an absorbed power-law model with $\Gamma = 1.1$ and a 0.3–10 keV X-ray flux of $3 \times 10^{-13}$ erg s$^{-1}$ cm$^{-2}$. Its black widow-like MSP nature was discovered after optical follow-up of the detected X-ray variable *Chandra* source revealed a 4.63 hr period of the binary derived via optical photometric (Kong et al. 2012) and spectroscopic (Romani & Shaw 2011) monitoring. In our *Chandra* observations, we found only one faint X-ray source (CXOU J165337.2−020020, N37) within the 0FGL J1653.4−0200 error ellipse to be possibly variable, albeit with limited statistics. In the case of CXOU J131145.7−343030, the bright source within the 2FGL ellipse of 0FGL J1311.9−3419 that had a *Suzaku* discovered short-term flare (factor of 10 increase in the first 20 ks of the ∼100 ks observation span), we found no significant variability within our 20 ks *Chandra* observation. However, these observations together with a *Swift* snapshot, provided evidence for variability on months' timescales also (Section 2.2). In this context, it may be fruitful to photometrically monitor the optical counterparts to these X-ray sources (Section 2.2) for similar variability as in the case of CXOU J233938.7−053305.

## 4. SUMMARY

*Chandra* observations of the two brightest unidentified high Galactic latitude $\gamma$-ray sources from the three-month *Fermi*-LAT bright source list were obtained. Both sources were previously detected by EGRET, and remain two of the most enigmatic $\gamma$-ray sources to date. The basic X-ray properties of all sources observed in the ACIS-I FOV were determined, with 9–13 X-ray sources detected within the respective *Fermi*-LAT error ellipses. Using existing catalogs (USNO B1.0, 2MASS, and *WISE*), the subarcsecond *Chandra* positions enabled us to locate optical, near-infrared, and mid-infrared counterparts to several of the X-ray sources. The ensemble of X-ray sources, focused primarily on the ones within the *Fermi*-LAT localizations, were further discussed as potential counterparts of the $\gamma$-ray sources. Although existing all-sky optical/infrared catalogs returned only a handful of X-ray counterpart matches, our work enables future optical identifications if deeper images can be obtained.

In the case of 0FGL J1311.9−3419, the brightest X-ray source (CXOU J131145.7−343030) within the *Fermi*-LAT error ellipse is the most credible counterpart. This source was detected in a previous *Suzaku* observation with X-ray variability on sub-day timescales, and our newly presented *Chandra* (and *Swift*) observations suggest variability on longer timescales. Together with the power-law nature of the X-ray spectrum, it appears similar to the case of CXOU J233938.7−053305, a candidate black widow MSP that is the likely counterpart of a similar

[14] To ease comparison with other works (see, e.g., Marelli et al. 2011), we extrapolated our 0.5–8 keV X-ray fluxes ($F_{0.5\text{–}8\,\mathrm{keV}}$) into 0.3–10 keV X-ray ones ($F_X$) assuming, $F_X = 1.25 \times F_{0.5\text{–}8\,\mathrm{keV}}$.

**Table 5**
All X-Ray Sources Found in the Field of the Four ACIS-I Chips in the *Chandra* Observation of 0FGL J1311.9−3419

| *N* | CXOU J Name | R.A. (deg) | Decl. (deg) | $r$ ($''$) | $D$ ($'$) | $A_{\rm eff}$ (cm$^2$) | log $P_{\rm K-S}$ | Counts (0.5–8 keV) | $\sigma$ | $P_{\rm B}$ | Counts (0.5–2 keV) | $\sigma$ | $P_{\rm B}$ | Counts (2–8 keV) | $\sigma$ | $P_{\rm B}$ |
|---|---|---|---|---|---|---|---|---|---|---|---|---|---|---|---|---|
| 1 | 131105.8−342652 | 197.77440 | −34.44785 | 1.36 | 9.7 | 401 | −0.31 | 10.4 +5.0/−3.8 | 2.1 | 1.4e-04 | 6.3 +4.0/−2.8 | 1.6 | 5.3e-04 | 4.1 +3.8/−2.6 | 1.1 | 3.4e-02 |
| 2 | 131108.7−342738 | 197.78660 | −34.46072 | 0.93 | 8.9 | 414 | −0.12 | 17.9 +5.7/−4.6 | 3.1 | 9.3e-11 | 7.9 +4.1/−2.9 | 1.9 | 7.1e-06 | 10.0 +4.6/−3.4 | 2.2 | 2.5e-06 |
| 3 | 131111.7−342856 | 197.79906 | −34.48245 | 1.26 | 8.2 | 390 | −0.00 | 6.7 +4.1/−2.9 | 1.6 | 8.4e-04 | 4.3 +3.4/−2.2 | 1.2 | 1.3e-03 | 2.4 +3.2/−1.9 | 0.8 | 8.1e-02 |
| 4 | 131112.2−343022 | 197.80102 | −34.50632 | 0.65 | 8.2 | 437 | −0.16 | 26.5 +6.5/−5.4 | 4.1 | 6.0e-20 | 14.1 +5.0/−3.8 | 2.8 | 6.4e-13 | 12.4 +4.8/−3.7 | 2.6 | 5.3e-09 |
| 5 | 131116.4−343147 | 197.81843 | −34.52992 | 0.99 | 7.7 | 439 | −0.56 | 9.1 +4.4/−3.3 | 2.0 | 8.8e-06 | 6.2 +3.8/−2.6 | 1.6 | 4.6e-05 | 2.9 +3.2/−1.9 | 0.9 | 2.7e-02 |
| 6 | 131118.0−342952 | 197.82502 | −34.49800 | 0.54 | 6.9 | 447 | −0.02 | 19.0 +5.6/−4.4 | 3.4 | 1.1e-18 | 11.7 +4.6/−3.4 | 2.5 | 1.6e-14 | 7.3 +4.0/−2.8 | 1.9 | 1.0e-06 |
| 7 | 131118.1−343013 | 197.82542 | −34.50362 | 0.81 | 6.9 | 449 | −0.08 | 8.9 +4.3/−3.1 | 2.1 | 5.7e-07 | 3.6 +3.2/−1.9 | 1.1 | 6.3e-04 | 5.2 +3.6/−2.4 | 1.4 | 2.2e-04 |
| 8 | 131119.6−342935 | 197.83179 | −34.49324 | 1.21 | 6.6 | 454 | −0.48 | 3.1 +3.2/−1.9 | 1.0 | 1.5e-02 | −0.3 +1.9/0.0 | −0.2 | 1.0 | 3.4 +3.2/−1.9 | 1.1 | 3.7e-03 |
| 9 | 131122.0−342744 | 197.84203 | −34.46232 | 1.07 | 6.2 | 388 | −0.78 | 3.1 +3.2/−1.9 | 1.0 | 1.3e-02 | 2.7 +2.9/−1.6 | 0.9 | 4.8e-03 | 0.4 +2.3/−0.8 | 0.2 | 4.4e-01 |
| 10 | 131125.5−342726 | 197.85662 | −34.45749 | 0.73 | 5.6 | 388 | −0.25 | 4.6 +3.4/−2.2 | 1.3 | 1.0e-04 | 0.8 +2.3/−0.8 | 0.4 | 1.5e-01 | 3.7 +3.2/−1.9 | 1.2 | 2.3e-04 |
| 11 | 131126.8−343428 | 197.86202 | −34.57448 | 1.40 | 7.3 | 455 | −0.76 | 3.3 +3.4/−2.2 | 1.0 | 3.3e-02 | −0.5 +1.9/0.0 | −0.3 | 1.0 | 3.8 +3.4/−2.2 | 1.1 | 8.8e-03 |
| 12 | 131126.9−343350 | 197.86211 | −34.56416 | 0.75 | 6.9 | 461 | −0.88 | 11.6 +4.7/−3.6 | 2.5 | 4.8e-09 | 9.4 +4.3/−3.1 | 2.2 | 2.4e-09 | 2.2 +2.9/−1.6 | 0.8 | 4.5e-02 |
| 13 | 131129.4−343133 | 197.87262 | −34.52597 | 0.69 | 5.1 | 483 | −0.22 | 4.5 +3.4/−2.2 | 1.3 | 1.4e-04 | −0.2 +1.9/0.0 | −0.1 | 1.0 | 4.7 +3.4/−2.2 | 1.4 | 2.2e-05 |
| 14 | 131131.4−343415 | 197.88124 | −34.57095 | 1.07 | 6.5 | 451 | −0.04 | 4.7 +3.6/−2.4 | 1.3 | 2.7e-03 | 4.6 +3.4/−2.2 | 1.4 | 6.9e-05 | 0.1 +2.3/−0.8 | 0.0 | 6.1e-01 |
| 15 | 131131.8−342546 | 197.88264 | −34.42969 | 0.78 | 5.3 | 457 | −0.03 | 3.4 +3.2/−1.9 | 1.1 | 3.2e-03 | 1.8 +2.7/−1.3 | 0.7 | 1.7e-02 | 1.6 +2.7/−1.3 | 0.6 | 6.2e-02 |
| 16 | 131133.7−342251 | 197.89081 | −34.38105 | 1.53 | 7.3 | 419 | −0.56 | 2.5 +3.4/−2.2 | 0.7 | 1.1e-01 | −0.8 +1.9/0.0 | −0.4 | 1.0 | 3.4 +3.4/−2.2 | 1.0 | 2.9e-02 |
| 17 | 131133.9−343331 | 197.89154 | −34.55871 | 1.07 | 5.6 | 443 | ... | 2.4 +2.9/−1.6 | 0.8 | 2.4e-02 | 2.8 +2.9/−1.6 | 0.9 | 1.4e-03 | −0.4 +1.9/0.0 | −0.2 | 1.0 |
| 18 | 131134.3−342303 | 197.89296 | −34.38430 | 1.14 | 7.1 | 424 | −0.06 | 5.0 +3.8/−2.6 | 1.3 | 5.1e-03 | 2.4 +2.9/−1.6 | 0.8 | 3.1e-02 | 2.6 +3.2/−1.9 | 0.8 | 5.2e-02 |
| 19 | 131134.3−342756 | 197.89323 | −34.46568 | 0.18 | 3.7 | 387 | −0.34 | 21.9 +5.8/−4.7 | 3.8 | 0.0 | 14.9 +5.0/−3.8 | 3.0 | 2.5e-30 | 6.9 +3.8/−2.6 | 1.8 | 1.5e-11 |
| 20 | 131134.3−342921 | 197.89332 | −34.48929 | 0.45 | 3.5 | 487 | ... | 2.9 +2.9/−1.6 | 1.0 | 2.5e-04 | 3.0 +2.9/−1.6 | 1.0 | 1.5e-05 | −0.1 +1.9/0.0 | 0.0 | 1.0 |
| 21 | 131134.7−343624 | 197.89495 | −34.60690 | 1.00 | 8.0 | 412 | −0.69 | 9.8 +4.6/−3.4 | 2.1 | 4.7e-06 | 1.1 +2.7/−1.3 | 0.4 | 2.3e-01 | 8.7 +4.3/−3.1 | 2.0 | 1.9e-06 |
| 22 | 131135.2−342824 | 197.89707 | −34.47335 | 0.37 | 3.4 | 487 | −0.98 | 3.9 +3.2/−1.9 | 1.2 | 1.1e-05 | 4.0 +3.2/−1.9 | 1.2 | 1.9e-07 | −0.1 +1.9/0.0 | 0.0 | 1.0 |
| 23 | 131135.6−342757 | 197.89835 | −34.46605 | 0.39 | 3.5 | 436 | −0.21 | 3.9 +3.2/−1.9 | 1.2 | 1.4e-05 | 3.0 +2.9/−1.6 | 1.0 | 1.9e-05 | 0.9 +2.3/−0.8 | 0.4 | 8.6e-02 |
| 24 | 131135.6−342710 | 197.89852 | −34.45300 | 0.52 | 3.8 | 471 | ... | 2.8 +2.9/−1.6 | 1.0 | 6.5e-04 | −0.1 +1.9/0.0 | 0.0 | 1.0 | 2.9 +2.9/−1.6 | 1.0 | 1.7e-04 |
| 25 | 131138.2−342605 | 197.90937 | −34.43479 | 0.50 | 4.1 | 432 | −0.15 | 3.8 +3.2/−1.9 | 1.2 | 7.6e-05 | 0.9 +2.3/−0.8 | 0.4 | 6.4e-02 | 2.9 +2.9/−1.6 | 1.0 | 5.1e-04 |
| 26 | 131139.3−342829 | 197.91403 | −34.47494 | 0.23 | 2.6 | 489 | −0.16 | 5.9 +3.6/−2.4 | 1.6 | 2.5e-10 | 4.0 +3.2/−1.9 | 1.2 | 1.2e-08 | 1.9 +2.7/−1.3 | 0.7 | 1.4e-03 |
| 27 | 131140.0−343023 | 197.91700 | −34.50657 | 0.30 | 2.6 | 495 | −1.85 | 3.9 +3.2/−1.9 | 1.2 | 1.3e-06 | 2.0 +2.7/−1.3 | 0.8 | 1.7e-04 | 1.9 +2.7/−1.3 | 0.7 | 1.6e-03 |
| 28 | 131141.1−343301 | 197.92156 | −34.55055 | 0.66 | 4.4 | 491 | ... | 2.7 +2.9/−1.6 | 0.9 | 3.2e-03 | −0.1 +1.9/0.0 | −0.1 | 1.0 | 2.8 +2.9/−1.6 | 1.0 | 9.6e-04 |
| 29 | 131141.9−342955 | 197.92481 | −34.49881 | 0.19 | 2.1 | 501 | −0.25 | 6.9 +3.8/−2.6 | 1.8 | 4.4e-13 | 1.0 +2.3/−0.8 | 0.4 | 1.8e-02 | 6.0 +3.6/−2.4 | 1.7 | 6.3e-12 |
| 30 | 131143.3−342826 | 197.93042 | −34.47410 | 0.27 | 1.8 | 473 | ... | 2.9 +2.9/−1.6 | 1.0 | 2.9e-05 | 0.0 +1.9/0.0 | 0.0 | 1.0 | 3.0 +2.9/−1.6 | 1.0 | 1.0e-05 |
| 31 | 131143.7−342749 | 197.93212 | −34.46388 | 0.26 | 2.1 | 497 | −1.48 | 3.9 +3.2/−1.9 | 1.2 | 2.1e-06 | 3.0 +2.9/−1.6 | 1.0 | 7.3e-06 | 0.9 +2.3/−0.8 | 0.4 | 4.9e-02 |
| 32 | 131143.9−342500 | 197.93320 | −34.41678 | 0.26 | 4.5 | 425 | −0.40 | 18.7 +5.4/−4.3 | 3.4 | 7.5e-27 | 6.9 +3.8/−2.6 | 1.8 | 7.8e-11 | 11.8 +4.6/−3.4 | 2.6 | 2.0e-17 |
| 33 | 131144.6−343100 | 197.93619 | −34.51691 | 0.24 | 2.3 | 500 | −0.28 | 4.9 +3.4/−2.2 | 1.4 | 1.9e-08 | 2.0 +2.7/−1.3 | 0.7 | 3.1e-04 | 3.0 +2.9/−1.6 | 1.0 | 2.1e-05 |

**Table 5**
(Continued)

| *N* | CXOU J Name | R.A. (deg) | Decl. (deg) | $r$ ($''$) | $D$ ($'$) | $A_{\rm eff}$ (cm$^2$) | log $P_{\rm K-S}$ | Counts (0.5–8 keV) | $\sigma$ | $P_{\rm B}$ | Counts (0.5–2 keV) | $\sigma$ | $P_{\rm B}$ | Counts (2–8 keV) | $\sigma$ | $P_{\rm B}$ |
|---|---|---|---|---|---|---|---|---|---|---|---|---|---|---|---|---|
| 34 | 131145.6−343313 | 197.94042 | −34.55386 | 0.43 | 4.2 | 447 | −1.66 | 5.7 +3.6/−2.4 | 1.6 | 4.0e-07 | 1.9 +2.7/−1.3 | 0.7 | 3.5e-03 | 3.8 +3.2/−1.9 | 1.2 | 3.9e-05 |
| 35 | 131145.7−343030 | 197.94049 | −34.50848 | 0.07 | 1.8 | 215 | −0.22 | 54.0 +8.4/−7.3 | 6.4 | 0.0 | 32.0 +6.7/−5.6 | 4.8 | 0.0 | 22.0 +5.8/−4.7 | 3.8 | 0.0 |
| 36 | 131146.0−342424 | 197.94207 | −34.40688 | 0.39 | 4.9 | 433 | −0.03 | 11.6 +4.6/−3.4 | 2.5 | 1.2e-13 | 9.8 +4.3/−3.1 | 2.3 | 2.2e-14 | 1.7 +2.7/−1.3 | 0.7 | 2.9e-02 |
| 37 | 131146.3−343259 | 197.94310 | −34.54985 | 0.55 | 3.9 | 452 | ... | 2.8 +2.9/−1.6 | 0.9 | 1.8e-03 | 1.9 +2.7/−1.3 | 0.7 | 3.0e-03 | 0.8 +2.3/−0.8 | 0.4 | 1.5e-01 |
| 38 | 131146.4−343050 | 197.94346 | −34.51394 | 0.18 | 1.9 | 506 | −0.02 | 7.9 +4.0/−2.8 | 2.0 | 1.3e-14 | 2.0 +2.7/−1.3 | 0.7 | 2.8e-04 | 6.0 +3.6/−2.4 | 1.7 | 1.3e-11 |
| 39 | 131147.0−343205 | 197.94600 | −34.53480 | 0.06 | 3.0 | 430 | −0.37 | 113.9 +11.7/−10.7 | 9.7 | 0.0 | 61.0 +8.9/−7.8 | 6.9 | 0.0 | 52.9 +8.3/−7.3 | 6.3 | 0.0 |
| 40 | 131147.0−342953 | 197.94607 | −34.49825 | 0.21 | 1.1 | 504 | −0.21 | 4.0 +3.2/−1.9 | 1.2 | 1.9e-07 | 3.0 +2.9/−1.6 | 1.0 | 4.9e-07 | 1.0 +2.3/−0.8 | 0.4 | 3.2e-02 |
| 41 | 131148.6−343729 | 197.95259 | −34.62488 | 1.11 | 8.3 | 445 | −0.04 | 7.7 +4.4/−3.3 | 1.7 | 8.6e-04 | 2.7 +3.2/−1.9 | 0.8 | 4.9e-02 | 5.0 +3.8/−2.6 | 1.3 | 5.6e-03 |
| 42 | 131149.0−342829 | 197.95455 | −34.47476 | 0.23 | 0.9 | 406 | ... | 3.0 +2.9/−1.6 | 1.0 | 7.8e-06 | 1.0 +2.3/−0.8 | 0.4 | 1.5e-02 | 2.0 +2.7/−1.3 | 0.7 | 2.3e-04 |
| 43 | 131149.2−343817 | 197.95519 | −34.63808 | 0.77 | 9.1 | 432 | −0.32 | 27.3 +6.7/−5.6 | 4.0 | 1.9e-15 | 20.4 +5.8/−4.7 | 3.5 | 3.0e-16 | 6.9 +4.3/−3.1 | 1.6 | 2.0e-03 |
| 44 | 131149.4−342607 | 197.95624 | −34.43547 | 0.35 | 3.1 | 445 | −0.94 | 3.9 +3.2/−1.9 | 1.2 | 7.5e-06 | 2.9 +2.9/−1.6 | 1.0 | 2.3e-05 | 0.9 +2.3/−0.8 | 0.4 | 6.5e-02 |
| 45 | 131149.6−343330 | 197.95677 | −34.55853 | 0.65 | 4.3 | 493 | ... | 2.7 +2.9/−1.6 | 0.9 | 3.2e-03 | −0.1 +1.9/0.0 | −0.1 | 1.0 | 2.8 +2.9/−1.6 | 1.0 | 9.7e-04 |
| 46 | 131150.1−343743 | 197.95910 | −34.62888 | 1.33 | 8.5 | 441 | −0.06 | 6.4 +4.3/−3.1 | 1.5 | 5.3e-03 | 2.7 +3.2/−1.9 | 0.9 | 4.6e-02 | 3.6 +3.6/−2.4 | 1.0 | 3.8e-02 |
| 47 | 131150.5−343029 | 197.96059 | −34.50809 | 0.23 | 1.3 | 483 | −0.04 | 3.9 +3.2/−1.9 | 1.2 | 3.5e-07 | 3.0 +2.9/−1.6 | 1.0 | 1.9e-06 | 1.0 +2.3/−0.8 | 0.4 | 3.2e-02 |
| 48 | 131152.1−342432 | 197.96709 | −34.40897 | 0.54 | 4.7 | 428 | −1.17 | 4.6 +3.4/−2.2 | 1.4 | 3.9e-05 | 2.8 +2.9/−1.6 | 1.0 | 6.8e-04 | 1.8 +2.7/−1.3 | 0.7 | 1.7e-02 |
| 49 | 131153.3−343212 | 197.97224 | −34.53684 | 0.27 | 3.0 | 475 | −1.44 | 6.9 +3.8/−2.6 | 1.8 | 7.3e-11 | 7.0 +3.8/−2.6 | 1.8 | 1.8e-13 | −0.1 +1.9/0.0 | 0.0 | 1.0 |
| 50 | 131153.5−342528 | 197.97325 | −34.42462 | 0.50 | 3.7 | 468 | ... | 2.8 +2.9/−1.6 | 1.0 | 8.2e-04 | 2.0 +2.7/−1.3 | 0.7 | 1.1e-03 | 0.9 +2.3/−0.8 | 0.4 | 1.2e-01 |
| 51 | 131154.3−343224 | 197.97630 | −34.54024 | 0.46 | 3.3 | 434 | ... | 2.9 +2.9/−1.6 | 1.0 | 3.9e-04 | 0.9 +2.3/−0.8 | 0.4 | 5.5e-02 | 1.9 +2.7/−1.3 | 0.7 | 3.2e-03 |
| 52 | 131154.3−342434 | 197.97658 | −34.40946 | 0.68 | 4.7 | 237 | ... | 2.8 +2.9/−1.6 | 1.0 | 1.0e-03 | 0.9 +2.3/−0.8 | 0.4 | 7.8e-02 | 1.9 +2.7/−1.3 | 0.7 | 5.8e-03 |
| 53 | 131154.5−342719 | 197.97720 | −34.45538 | 0.29 | 2.0 | 477 | ... | 2.9 +2.9/−1.6 | 1.0 | 6.4e-05 | 0.0 +1.9/0.0 | 0.0 | 1.0 | 3.0 +2.9/−1.6 | 1.0 | 1.6e-05 |
| 54 | 131154.9−342642 | 197.97910 | −34.44522 | 0.34 | 2.6 | 483 | ... | 2.9 +2.9/−1.6 | 1.0 | 7.8e-05 | 2.0 +2.7/−1.3 | 0.7 | 4.9e-04 | 1.0 +2.3/−0.8 | 0.4 | 4.7e-02 |
| 55 | 131156.1−342126 | 197.98379 | −34.35747 | 1.22 | 7.8 | 386 | −0.71 | 6.2 +4.0/−2.8 | 1.6 | 6.2e-04 | 4.3 +3.4/−2.2 | 1.3 | 1.2e-03 | 2.0 +2.9/−1.6 | 0.7 | 9.3e-02 |
| 56 | 131156.2−342335 | 197.98440 | −34.39309 | 0.30 | 5.7 | 427 | −0.32 | 29.2 +6.5/−5.4 | 4.5 | 9.8e-35 | 19.8 +5.6/−4.4 | 3.6 | 1.4e-29 | 9.4 +4.3/−3.1 | 2.2 | 1.1e-09 |
| 57 | 131156.6−342055 | 197.98587 | −34.34866 | 0.49 | 8.3 | 252 | −0.04 | 20.3 +5.8/−4.7 | 3.5 | 3.4e-13 | 17.2 +5.3/−4.2 | 3.2 | 3.6e-13 | 3.1 +3.2/−1.9 | 1.0 | 2.8e-02 |
| 58 | 131156.7−343045 | 197.98631 | −34.51257 | 0.12 | 1.9 | 507 | −0.11 | 18.9 +5.4/−4.3 | 3.5 | 0.0 | 13.0 +4.7/−3.6 | 2.8 | 1.6e-30 | 6.0 +3.6/−2.4 | 1.6 | 2.4e-11 |
| 59 | 131156.8−342403 | 197.98691 | −34.40101 | 1.17 | 5.3 | 457 | ... | 1.4 +2.7/−1.3 | 0.5 | 1.2e-01 | 1.8 +2.7/−1.3 | 0.7 | 2.3e-02 | −0.4 +1.9/0.0 | −0.2 | 1.0 |
| 60 | 131157.1−342055 | 197.98814 | −34.34882 | 0.91 | 8.4 | 166 | ... | 1.8 +2.9/−1.6 | 0.6 | 1.3e-01 | 0.2 +2.3/−0.8 | 0.1 | 5.5e-01 | 1.6 +2.7/−1.3 | 0.6 | 7.7e-02 |
| 61 | 131158.2−342734 | 197.99275 | −34.45946 | 0.19 | 2.2 | 458 | −0.75 | 6.9 +3.8/−2.6 | 1.8 | 1.2e-12 | 4.0 +3.2/−1.9 | 1.2 | 1.6e-08 | 3.0 +2.9/−1.6 | 1.0 | 1.3e-05 |
| 62 | 131159.2−342955 | 197.99670 | −34.49864 | 0.25 | 1.8 | 457 | −1.82 | 3.9 +3.2/−1.9 | 1.2 | 5.5e-07 | 4.0 +3.2/−1.9 | 1.2 | 8.4e-09 | 0.0 +1.9/0.0 | 0.0 | 1.0 |
| 63 | 131159.2−343133 | 197.99692 | −34.52606 | 0.22 | 2.9 | 465 | −0.02 | 9.9 +4.3/−3.1 | 2.3 | 2.9e-17 | 1.0 +2.3/−0.8 | 0.4 | 4.0e-02 | 8.9 +4.1/−2.9 | 2.2 | 3.2e-17 |
| 64 | 131159.5−343555 | 197.99810 | −34.59878 | 0.35 | 6.9 | 424 | −0.02 | 52.4 +8.4/−7.3 | 6.2 | 0.0 | 35.4 +7.1/−6.0 | 5.0 | 0.0 | 17.0 +5.3/−4.2 | 3.2 | 6.4e-16 |
| 65 | 131200.4−343231 | 198.00170 | −34.54213 | 0.17 | 3.8 | 461 | −0.00 | 33.7 +6.9/−5.8 | 4.9 | 0.0 | 22.9 +5.9/−4.8 | 3.9 | 0.0 | 10.8 +4.4/−3.3 | 2.4 | 4.9e-16 |
| 66 | 131202.0−343234 | 198.00857 | −34.54281 | 0.22 | 4.0 | 459 | −0.03 | 22.7 +5.9/−4.8 | 3.9 | 7.7e-35 | 5.9 +3.6/−2.4 | 1.6 | 1.7e-09 | 16.8 +5.2/−4.1 | 3.2 | 7.0e-27 |

**Table 5**
(Continued)

| *N* | CXOU J Name | R.A. (deg) | Decl. (deg) | *r* (″) | *D* (′) | $A_{\rm eff}$ (cm$^2$) | log $P_{\rm K-S}$ | Counts (0.5–8 keV) | $\sigma$ | $P_{\rm B}$ | Counts (0.5–2 keV) | $\sigma$ | $P_{\rm B}$ | Counts (2–8 keV) | $\sigma$ | $P_{\rm B}$ |
|---|---|---|---|---|---|---|---|---|---|---|---|---|---|---|---|---|
| 67 | 131202.5−342835 | 198.01065 | −34.47657 | 0.34 | 2.4 | 461 | ... | 2.9 +2.9/−1.6 | 1.0 | 1.3e-04 | 2.0 +2.7/−1.3 | 0.7 | 8.1e-04 | 0.9 +2.3/−0.8 | 0.4 | 5.2e-02 |
| 68 | 131202.9−342539 | 198.01213 | −34.42761 | 0.52 | 4.3 | 473 | −0.01 | 3.8 +3.2/−1.9 | 1.2 | 1.0e-04 | 2.9 +2.9/−1.6 | 1.0 | 7.6e-05 | 0.8 +2.3/−0.8 | 0.4 | 1.4e-01 |
| 69 | 131203.9−342026 | 198.01630 | −34.34067 | 0.76 | 9.1 | 372 | −0.76 | 27.1 +6.6/−5.5 | 4.1 | 1.4e-16 | 27.9 +6.5/−5.4 | 4.3 | 4.5e-27 | −0.9 +2.7/−1.3 | −0.3 | 7.8e-01 |
| 70 | 131203.9−343653 | 198.01636 | −34.61482 | 0.59 | 8.1 | 437 | −0.11 | 33.4 +7.2/−6.1 | 4.7 | 7.2e-23 | 18.9 +5.6/−4.4 | 3.4 | 6.9e-17 | 14.5 +5.2/−4.1 | 2.8 | 6.2e-09 |
| 71 | 131204.4−343559 | 198.01873 | −34.59985 | 1.11 | 7.3 | 451 | −0.27 | 5.9 +4.0/−2.8 | 1.5 | 1.9e-03 | −0.7 +1.9/0.0 | −0.4 | 1.0 | 6.6 +4.0/−2.8 | 1.7 | 1.5e-04 |
| 72 | 131205.2−342502 | 198.02176 | −34.41736 | 0.67 | 5.0 | 456 | −0.01 | 3.6 +3.2/−1.9 | 1.1 | 5.2e-04 | 0.9 +2.3/−0.8 | 0.4 | 1.3e-01 | 2.8 +2.9/−1.6 | 0.9 | 1.6e-03 |
| 73 | 131205.3−342813 | 198.02211 | −34.47039 | 0.36 | 3.0 | 485 | −0.68 | 3.9 +3.2/−1.9 | 1.2 | 1.2e-05 | 2.9 +2.9/−1.6 | 1.0 | 3.3e-05 | 0.9 +2.3/−0.8 | 0.4 | 7.3e-02 |
| 74 | 131205.6−343126 | 198.02371 | −34.52414 | 0.53 | 3.7 | 490 | ... | 2.8 +2.9/−1.6 | 0.9 | 1.8e-03 | −0.1 +1.9/0.0 | 0.0 | 1.0 | 2.8 +2.9/−1.6 | 1.0 | 5.7e-04 |
| 75 | 131206.1−343152 | 198.02560 | −34.53122 | 0.20 | 4.0 | 482 | −0.27 | 23.8 +6.0/−4.9 | 4.0 | 5.8e-38 | 16.9 +5.2/−4.1 | 3.2 | 1.8e-31 | 6.8 +3.8/−2.6 | 1.8 | 6.2e-10 |
| 76 | 131206.2−343449 | 198.02606 | −34.58041 | 0.44 | 6.4 | 457 | −1.40 | 26.7 +6.4/−5.3 | 4.2 | 3.1e-26 | 17.6 +5.3/−4.2 | 3.3 | 2.0e-21 | 9.1 +4.3/−3.1 | 2.1 | 4.8e-08 |
| 77 | 131206.5−342910 | 198.02731 | −34.48618 | 0.43 | 3.1 | 433 | ... | 2.9 +2.9/−1.6 | 1.0 | 2.3e-04 | 2.0 +2.7/−1.3 | 0.7 | 9.0e-04 | 0.9 +2.3/−0.8 | 0.4 | 6.9e-02 |
| 78 | 131207.4−343107 | 198.03086 | −34.51887 | 0.20 | 3.8 | 486 | −0.21 | 20.8 +5.7/−4.5 | 3.7 | 2.1e-34 | 13.9 +4.8/−3.7 | 2.9 | 3.6e-27 | 6.9 +3.8/−2.6 | 1.8 | 1.9e-10 |
| 79 | 131207.7−342622 | 198.03237 | −34.43961 | 0.65 | 4.4 | 445 | ... | 2.8 +2.9/−1.6 | 0.9 | 1.4e-03 | 1.9 +2.7/−1.3 | 0.7 | 2.7e-03 | 0.9 +2.3/−0.8 | 0.4 | 1.3e-01 |
| 80 | 131207.8−342938 | 198.03253 | −34.49399 | 0.47 | 3.4 | 483 | ... | 2.9 +2.9/−1.6 | 1.0 | 3.5e-04 | 1.0 +2.3/−0.8 | 0.4 | 4.8e-02 | 1.9 +2.7/−1.3 | 0.7 | 3.3e-03 |
| 81 | 131209.2−343622 | 198.03871 | −34.60625 | 0.58 | 8.1 | 440 | −0.10 | 34.2 +7.1/−6.1 | 4.8 | 9.1e-27 | 23.3 +6.0/−4.9 | 3.9 | 4.1e-25 | 11.0 +4.7/−3.6 | 2.3 | 5.2e-07 |
| 82 | 131209.8−343440 | 198.04118 | −34.57790 | 0.80 | 6.7 | 437 | −0.12 | 8.8 +4.3/−3.1 | 2.0 | 9.0e-07 | 7.5 +4.0/−2.8 | 1.9 | 6.5e-08 | 1.2 +2.7/−1.3 | 0.5 | 1.8e-01 |
| 83 | 131211.7−342558 | 198.04886 | −34.43281 | 0.68 | 5.3 | 424 | −0.35 | 4.6 +3.4/−2.2 | 1.4 | 5.8e-05 | −0.2 +1.9/0.0 | −0.1 | 1.0 | 4.8 +3.4/−2.2 | 1.4 | 4.3e-06 |
| 84 | 131217.8−342938 | 198.07458 | −34.49393 | 0.76 | 5.5 | 470 | −0.12 | 4.3 +3.4/−2.2 | 1.3 | 6.2e-04 | 3.8 +3.2/−1.9 | 1.2 | 1.1e-04 | 0.6 +2.3/−0.8 | 0.2 | 3.5e-01 |
| 85 | 131218.4−342819 | 198.07683 | −34.47197 | 0.57 | 5.6 | 373 | −0.05 | 9.4 +4.3/−3.1 | 2.2 | 1.2e-09 | 6.7 +3.8/−2.6 | 1.8 | 2.0e-08 | 2.7 +2.9/−1.6 | 0.9 | 5.1e-03 |
| 86 | 131219.5−342811 | 198.08141 | −34.46998 | 1.01 | 5.9 | 349 | −0.45 | 3.4 +3.2/−1.9 | 1.1 | 4.1e-03 | 0.8 +2.3/−0.8 | 0.3 | 2.2e-01 | 2.6 +2.9/−1.6 | 0.9 | 7.0e-03 |
| 87 | 131220.2−342931 | 198.08456 | −34.49205 | 1.01 | 6.0 | 459 | −0.10 | 3.2 +3.2/−1.9 | 1.0 | 1.0e-02 | 1.7 +2.7/−1.3 | 0.6 | 4.5e-02 | 1.5 +2.7/−1.3 | 0.6 | 8.8e-02 |
| 88 | 131220.4−343456 | 198.08521 | −34.58249 | 1.53 | 8.3 | 404 | −1.60 | 4.1 +3.8/−2.6 | 1.1 | 3.0e-02 | 4.1 +3.4/−2.2 | 1.2 | 3.4e-03 | 0.1 +2.7/−1.3 | 0.0 | 5.8e-01 |
| 89 | 131223.1−342912 | 198.09643 | −34.48689 | 0.34 | 6.5 | 448 | −1.70 | 39.8 +7.5/−6.4 | 5.3 | 0.0 | 29.5 +6.5/−5.4 | 4.5 | 0.0 | 10.3 +4.4/−3.3 | 2.3 | 5.4e-10 |
| 90 | 131224.5−342859 | 198.10229 | −34.48330 | 0.93 | 6.8 | 449 | −0.04 | 6.5 +4.0/−2.8 | 1.6 | 2.0e-04 | 3.4 +3.2/−1.9 | 1.1 | 4.2e-03 | 3.1 +3.2/−1.9 | 1.0 | 1.4e-02 |
| 91 | 131225.3−342501 | 198.10569 | −34.41703 | 0.78 | 8.1 | 404 | −0.81 | 19.7 +5.8/−4.7 | 3.4 | 6.4e-14 | 19.0 +5.6/−4.4 | 3.4 | 3.2e-18 | 0.6 +2.7/−1.3 | 0.2 | 4.0e-01 |
| 92 | 131225.5−342628 | 198.10644 | −34.44130 | 0.66 | 7.5 | 410 | −0.84 | 20.2 +5.8/−4.7 | 3.5 | 4.4e-16 | 13.2 +4.8/−3.7 | 2.7 | 6.2e-13 | 6.9 +4.0/−2.8 | 1.8 | 2.3e-05 |
| 93 | 131226.8−343029 | 198.11173 | −34.50825 | 1.26 | 7.4 | 411 | −0.40 | 4.2 +3.6/−2.4 | 1.2 | 1.1e-02 | 2.3 +2.9/−1.6 | 0.8 | 3.5e-02 | 1.9 +2.9/−1.6 | 0.7 | 1.0e-01 |
| 94 | 131228.3−343136 | 198.11798 | −34.52668 | 1.62 | 8.0 | 400 | −1.41 | 2.9 +3.4/−2.2 | 0.9 | 6.3e-02 | 4.2 +3.4/−2.2 | 1.2 | 2.1e-03 | −1.2 +1.9/0.0 | −0.7 | 1.0 |
| 95 | 131229.1−342641 | 198.12128 | −34.44483 | 0.56 | 8.2 | 236 | −1.72 | 37.5 +7.3/−6.2 | 5.1 | 3.4e-38 | 20.3 +5.7/−4.5 | 3.6 | 2.6e-22 | 17.2 +5.3/−4.2 | 3.2 | 1.5e-17 |
| 96 | 131234.9−342925 | 198.14571 | −34.49055 | 0.80 | 9.0 | 396 | −0.48 | 24.5 +6.4/−5.3 | 3.8 | 3.5e-15 | 20.8 +5.8/−4.7 | 3.6 | 2.8e-18 | 3.7 +3.6/−2.4 | 1.0 | 3.6e-02 |
| 97 | 131236.3−343004 | 198.15137 | −34.50131 | 0.83 | 9.3 | 416 | −0.19 | 25.4 +6.5/−5.4 | 3.9 | 7.9e-16 | 5.0 +3.6/−2.4 | 1.4 | 9.5e-04 | 20.4 +5.9/−4.8 | 3.5 | 1.4e-13 |

**Table 6**
All X-Ray Sources Found in the Field of the Four ACIS-I Chips in the *Chandra* Observation of 0FGL J1653.4−0200

| *N* | CXOU J Name | R.A. (deg) | Decl. (deg) | $r$ ($''$) | $D$ ($'$) | $A_{\rm eff}$ (cm$^2$) | log $P_{\rm K-S}$ | Counts (0.5–8 keV) | $\sigma$ | $P_{\rm B}$ | Counts (0.5–2 keV) | $\sigma$ | $P_{\rm B}$ | Counts (2–8 keV) | $\sigma$ | $P_{\rm B}$ |
|---|---|---|---|---|---|---|---|---|---|---|---|---|---|---|---|---|
| 1 | 165305.4−020127 | 253.27286 | −2.02433 | 1.84 | 10.2 | 394 | −0.13 | 5.1 +4.5/−3.3 | 1.1 | 4.3e-02 | 0.7 +3.0/−1.7 | 0.2 | 4.2e-01 | 4.4 +4.0/−2.8 | 1.1 | 3.3e-02 |
| 2 | 165307.6−015954 | 253.28203 | −1.99854 | 0.86 | 9.2 | 286 | −0.06 | 22.3 +6.2/−5.1 | 3.6 | 4.3e-13 | 7.3 +4.1/−2.9 | 1.8 | 1.1e-04 | 14.9 +5.2/−4.1 | 2.9 | 5.2e-10 |
| 3 | 165309.0−020138 | 253.28751 | −2.02737 | 0.68 | 9.4 | 410 | −0.10 | 40.3 +7.9/−6.8 | 5.1 | 2.7e-24 | 26.7 +6.5/−5.4 | 4.1 | 2.9e-20 | 13.6 +5.2/−4.1 | 2.6 | 3.1e-07 |
| 4 | 165309.7−015915 | 253.29050 | −1.98769 | 0.80 | 8.6 | 411 | −0.21 | 20.4 +6.0/−4.9 | 3.4 | 4.6e-12 | 14.6 +5.1/−4.0 | 2.9 | 1.5e-11 | 5.8 +4.0/−2.8 | 1.5 | 2.6e-03 |
| 5 | 165310.3−015926 | 253.29301 | −1.99058 | 0.99 | 8.5 | 373 | −0.29 | 9.7 +4.6/−3.4 | 2.1 | 7.5e-06 | 2.1 +2.9/−1.6 | 0.7 | 6.4e-02 | 7.6 +4.1/−2.9 | 1.8 | 2.4e-05 |
| 6 | 165312.4−015943 | 253.30206 | −1.99541 | 1.25 | 8.0 | 422 | −0.21 | 6.1 +4.1/−3.0 | 1.5 | 4.1e-03 | 3.9 +3.4/−2.2 | 1.2 | 5.9e-03 | 2.1 +3.2/−1.9 | 0.7 | 1.3e-01 |
| 7 | 165315.2−020314 | 253.31349 | −2.05407 | 0.96 | 8.9 | 420 | −0.18 | 14.2 +5.3/−4.2 | 2.7 | 2.9e-07 | 5.6 +3.8/−2.6 | 1.5 | 1.1e-03 | 8.6 +4.4/−3.3 | 1.9 | 6.7e-05 |
| 8 | 165315.6−015822 | 253.31502 | −1.97283 | 0.06 | 7.1 | 360 | −0.12 | 1674.0 +42.0/−40.9 | 39.9 | 0.0 | 1138.4 +34.8/−33.8 | 32.7 | 0.0 | 535.6 +24.2/−23.2 | 22.1 | 0.0 |
| 9 | 165318.2−020116 | 253.32620 | −2.02115 | 1.15 | 7.2 | 436 | −0.16 | 4.3 +3.6/−2.4 | 1.2 | 8.4e-03 | 1.4 +2.7/−1.3 | 0.5 | 1.1e-01 | 2.9 +3.2/−1.9 | 0.9 | 3.0e-02 |
| 10 | 165318.3−015927 | 253.32629 | −1.99097 | 1.08 | 6.5 | 444 | −1.41 | 3.6 +3.4/−2.2 | 1.1 | 1.5e-02 | −0.5 +1.9/0.0 | −0.3 | 1.0 | 4.1 +3.4/−2.2 | 1.2 | 2.6e-03 |
| 11 | 165318.4−015434 | 253.32693 | −1.90966 | 0.92 | 7.2 | 394 | −0.64 | 9.6 +4.6/−3.4 | 2.1 | 1.2e-05 | 6.0 +3.8/−2.6 | 1.6 | 1.3e-04 | 3.6 +3.4/−2.2 | 1.1 | 1.6e-02 |
| 12 | 165321.5−015703 | 253.33975 | −1.95102 | 0.75 | 5.7 | 393 | −0.07 | 5.0 +3.6/−2.4 | 1.4 | 6.1e-04 | −0.5 +1.9/0.0 | −0.2 | 1.0 | 5.5 +3.6/−2.4 | 1.5 | 2.2e-05 |
| 13 | 165323.1−015252 | 253.34642 | −1.88130 | 1.40 | 7.3 | 379 | −0.07 | 3.1 +3.4/−2.2 | 0.9 | 4.3e-02 | 3.4 +3.2/−1.9 | 1.1 | 4.5e-03 | −0.2 +2.3/−0.8 | −0.1 | 7.1e-01 |
| 14 | 165323.2−020451 | 253.34676 | −2.08089 | 0.38 | 8.6 | 335 | −1.42 | 89.4 +10.6/−9.6 | 8.4 | 0.0 | 59.2 +8.8/−7.7 | 6.7 | 0.0 | 30.2 +6.7/−5.6 | 4.5 | 8.8e-27 |
| 15 | 165323.2−015809 | 253.34687 | −1.96928 | 0.60 | 5.1 | 459 | −0.26 | 5.4 +3.6/−2.4 | 1.5 | 3.3e-05 | 1.8 +2.7/−1.3 | 0.7 | 2.1e-02 | 3.6 +3.2/−1.9 | 1.1 | 5.3e-04 |
| 16 | 165323.9−020155 | 253.34988 | −2.03222 | 1.13 | 6.3 | 454 | ... | 2.0 +2.9/−1.6 | 0.7 | 8.1e-02 | 2.7 +2.9/−1.6 | 0.9 | 5.0e-03 | −0.7 +1.9/0.0 | −0.4 | 1.0 |
| 17 | 165324.6−015932 | 253.35291 | −1.99234 | 0.40 | 5.0 | 375 | −0.03 | 10.5 +4.4/−3.3 | 2.4 | 4.8e-12 | 6.8 +3.8/−2.6 | 1.8 | 1.1e-09 | 3.7 +3.2/−1.9 | 1.2 | 2.6e-04 |
| 18 | 165325.7−015617 | 253.35745 | −1.93829 | 0.71 | 4.8 | 343 | −0.43 | 3.5 +3.2/−1.9 | 1.1 | 1.4e-03 | −0.2 +1.9/0.0 | −0.1 | 1.0 | 3.7 +3.2/−1.9 | 1.2 | 2.9e-04 |
| 19 | 165325.8−015107 | 253.35787 | −1.85215 | 0.70 | 8.2 | 357 | −1.04 | 23.4 +6.2/−5.1 | 3.8 | 1.3e-16 | 8.9 +4.3/−3.1 | 2.1 | 5.9e-07 | 14.5 +5.1/−4.0 | 2.8 | 3.9e-11 |
| 20 | 165325.9−015316 | 253.35808 | −1.88782 | 0.83 | 6.5 | 366 | −0.06 | 6.8 +4.0/−2.8 | 1.7 | 5.8e-05 | 4.7 +3.4/−2.2 | 1.4 | 3.6e-05 | 2.1 +2.9/−1.6 | 0.7 | 6.8e-02 |
| 21 | 165326.3−015502 | 253.35973 | −1.91743 | 0.84 | 5.3 | 417 | −0.14 | 3.3 +3.2/−1.9 | 1.0 | 7.2e-03 | 1.8 +2.7/−1.3 | 0.7 | 1.9e-02 | 1.5 +2.7/−1.3 | 0.6 | 1.0e-01 |
| 22 | 165326.9−015741 | 253.36237 | −1.96154 | 0.61 | 4.2 | 465 | ... | 2.7 +2.9/−1.6 | 0.9 | 4.0e-03 | 1.9 +2.7/−1.3 | 0.7 | 5.3e-03 | 0.8 +2.3/−0.8 | 0.3 | 1.9e-01 |
| 23 | 165327.4−015118 | 253.36437 | −1.85509 | 1.67 | 7.9 | 423 | −0.07 | 3.6 +3.6/−2.4 | 1.0 | 3.8e-02 | 4.0 +3.4/−2.2 | 1.2 | 4.8e-03 | −0.4 +2.3/−0.8 | −0.2 | 7.5e-01 |
| 24 | 165328.4−020009 | 253.36843 | −2.00261 | 0.28 | 4.4 | 471 | −0.02 | 13.7 +4.8/−3.7 | 2.8 | 1.7e-18 | 11.9 +4.6/−3.4 | 2.6 | 2.5e-19 | 1.8 +2.7/−1.3 | 0.7 | 1.5e-02 |
| 25 | 165330.0−015827 | 253.37516 | −1.97442 | 0.45 | 3.5 | 479 | ... | 2.8 +2.9/−1.6 | 1.0 | 6.6e-04 | 1.9 +2.7/−1.3 | 0.7 | 3.1e-03 | 0.9 +2.3/−0.8 | 0.4 | 8.1e-02 |
| 26 | 165331.4−020137 | 253.38113 | −2.02713 | 0.73 | 4.8 | 462 | ... | 2.6 +2.9/−1.6 | 0.9 | 6.8e-03 | −0.2 +1.9/0.0 | −0.1 | 1.0 | 2.8 +2.9/−1.6 | 0.9 | 1.3e-03 |
| 27 | 165332.8−015902 | 253.38701 | −1.98411 | 0.37 | 2.9 | 486 | ... | 2.9 +2.9/−1.6 | 1.0 | 3.1e-04 | 0.9 +2.3/−0.8 | 0.4 | 5.1e-02 | 1.9 +2.7/−1.3 | 0.7 | 2.7e-03 |
| 28 | 165333.5−015259 | 253.38978 | −1.88320 | 0.12 | 5.6 | 451 | −0.06 | 173.3 +14.2/−13.2 | 12.2 | 0.0 | 172.8 +14.2/−13.1 | 12.2 | 0.0 | 0.6 +2.3/−0.8 | 0.2 | 3.6e-01 |
| 29 | 165334.5−020230 | 253.39413 | −2.04180 | 0.38 | 5.1 | 476 | −0.34 | 13.5 +4.8/−3.7 | 2.8 | 2.5e-15 | 7.8 +4.0/−2.8 | 2.0 | 1.7e-10 | 5.7 +3.6/−2.4 | 1.6 | 1.6e-06 |
| 30 | 165334.8−020031 | 253.39522 | −2.00879 | 0.43 | 3.4 | 491 | ... | 2.9 +2.9/−1.6 | 1.0 | 4.8e-04 | −0.1 +1.9/0.0 | 0.0 | 1.0 | 2.9 +2.9/−1.6 | 1.0 | 1.1e-04 |
| 31 | 165334.8−015803 | 253.39522 | −1.96760 | 0.23 | 2.2 | 485 | −0.31 | 4.9 +3.4/−2.2 | 1.4 | 1.2e-08 | 3.0 +2.9/−1.6 | 1.0 | 2.1e-06 | 2.0 +2.7/−1.3 | 0.7 | 1.0e-03 |
| 32 | 165334.9−020317 | 253.39542 | −2.05488 | 0.87 | 5.7 | 470 | −0.25 | 4.1 +3.4/−2.2 | 1.2 | 2.7e-03 | 0.6 +2.3/−0.8 | 0.3 | 3.3e-01 | 3.5 +3.2/−1.9 | 1.1 | 2.2e-03 |
| 33 | 165336.3−014918 | 253.40146 | −1.82192 | 0.36 | 8.9 | 358 | −0.06 | 101.7 +11.3/−10.3 | 9.0 | 0.0 | 68.9 +9.5/−8.4 | 7.3 | 0.0 | 32.8 +7.0/−5.9 | 4.7 | 3.4e-26 |

**Table 6**
(Continued)

| N | CXOU J Name | R.A. (deg) | Decl. (deg) | r (″) | D (′) | $A_{\rm eff}$ ($\rm cm^2$) | log $P_{\rm K-S}$ | Counts (0.5–8 keV) | σ | $P_{\rm B}$ | Counts (0.5–2 keV) | σ | $P_{\rm B}$ | Counts (2–8 keV) | σ | $P_{\rm B}$ |
|---|---|---|---|---|---|---|---|---|---|---|---|---|---|---|---|---|
| 34 | 165336.7−014907 | 253.40294 | −1.81872 | 0.60 | 9.1 | 216 | −0.01 | 14.5 +5.1/−4.0 | 2.9 | 9.5e-12 | 7.3 +4.0/−2.8 | 1.8 | 1.3e-06 | 7.3 +4.0/−2.8 | 1.8 | 1.6e-06 |
| 35 | 165337.0−020211 | 253.40424 | −2.03646 | 0.49 | 4.5 | 481 | −0.77 | 5.6 +3.6/−2.4 | 1.6 | 3.3e-06 | 4.8 +3.4/−2.2 | 1.4 | 8.3e-07 | 0.8 +2.3/−0.8 | 0.3 | 2.0e-01 |
| 36 | 165337.1−020442 | 253.40491 | −2.07841 | 0.76 | 6.9 | 420 | −0.16 | 10.5 +4.6/−3.4 | 2.3 | 1.2e-07 | 4.4 +3.4/−2.2 | 1.3 | 5.1e-04 | 6.1 +3.8/−2.6 | 1.6 | 6.1e-05 |
| 37 | 165337.2−020020 | 253.40519 | −2.00568 | 0.18 | 2.9 | 491 | −1.92 | 11.9 +4.6/−3.4 | 2.6 | 3.8e-21 | 5.0 +3.4/−2.2 | 1.5 | 1.4e-09 | 6.9 +3.8/−2.6 | 1.8 | 6.6e-13 |
| 38 | 165338.0−015836 | 253.40855 | −1.97685 | 0.03 | 1.6 | 500 | −0.37 | 306.9 +18.5/−17.5 | 16.6 | 0.0 | 198.0 +15.1/−14.1 | 13.1 | 0.0 | 109.0 +11.5/−10.4 | 9.5 | 0.0 |
| 39 | 165338.9−015007 | 253.41248 | −1.83532 | 1.09 | 8.0 | 330 | −0.43 | 8.0 +4.3/−3.1 | 1.9 | 6.1e-05 | −0.9 +1.9/0.0 | −0.5 | 1.0 | 8.9 +4.3/−3.1 | 2.1 | 6.0e-07 |
| 40 | 165339.1−015412 | 253.41314 | −1.90339 | 0.54 | 4.0 | 469 | ... | 2.8 +2.9/−1.6 | 0.9 | 1.4e-03 | −0.1 +1.9/0.0 | 0.0 | 1.0 | 2.9 +2.9/−1.6 | 1.0 | 4.6e-04 |
| 41 | 165339.4−015051 | 253.41434 | −1.84757 | 0.98 | 7.2 | 361 | −0.79 | 6.5 +4.0/−2.8 | 1.6 | 1.8e-04 | 5.4 +3.6/−2.4 | 1.5 | 4.5e-05 | 1.1 +2.7/−1.3 | 0.4 | 2.3e-01 |
| 42 | 165339.6−015033 | 253.41537 | −1.84275 | 0.83 | 7.5 | 339 | −0.73 | 10.5 +4.6/−3.4 | 2.3 | 8.8e-08 | 5.4 +3.6/−2.4 | 1.5 | 4.9e-05 | 5.1 +3.6/−2.4 | 1.4 | 3.7e-04 |
| 43 | 165340.3−015329 | 253.41809 | −1.89151 | 0.69 | 4.6 | 464 | ... | 2.6 +2.9/−1.6 | 0.9 | 6.3e-03 | 2.9 +2.9/−1.6 | 1.0 | 5.6e-04 | −0.2 +1.9/0.0 | −0.1 | 1.0 |
| 44 | 165341.4−015927 | 253.42251 | −1.99084 | 0.10 | 1.6 | 504 | −1.12 | 18.9 +5.4/−4.3 | 3.5 | 0.0 | 17.0 +5.2/−4.1 | 3.3 | 0.0 | 2.0 +2.7/−1.3 | 0.7 | 8.0e-04 |
| 45 | 165341.4−020451 | 253.42281 | −2.08095 | 1.26 | 6.9 | 460 | −0.10 | 3.6 +3.4/−2.2 | 1.1 | 1.6e-02 | 3.5 +3.2/−1.9 | 1.1 | 2.8e-03 | 0.1 +2.3/−0.8 | 0.1 | 5.8e-01 |
| 46 | 165341.6−015425 | 253.42350 | −1.90709 | 0.42 | 3.6 | 478 | −0.47 | 3.8 +3.2/−1.9 | 1.2 | 5.4e-05 | 0.9 +2.3/−0.8 | 0.4 | 7.3e-02 | 2.9 +2.9/−1.6 | 1.0 | 2.8e-04 |
| 47 | 165342.4−020034 | 253.42708 | −2.00949 | 0.36 | 2.6 | 223 | ... | 3.0 +2.9/−1.6 | 1.0 | 1.2e-05 | 2.0 +2.7/−1.3 | 0.8 | 1.5e-04 | 1.0 +2.3/−0.8 | 0.4 | 2.4e-02 |
| 48 | 165342.6−020516 | 253.42769 | −2.08805 | 1.25 | 7.3 | 418 | −0.18 | 4.3 +3.6/−2.4 | 1.2 | 9.0e-03 | 4.4 +3.4/−2.2 | 1.3 | 5.4e-04 | −0.1 +2.3/−0.8 | 0.0 | 6.7e-01 |
| 49 | 165342.8−020144 | 253.42846 | −2.02914 | 0.38 | 3.7 | 452 | −0.35 | 5.8 +3.6/−2.4 | 1.6 | 1.1e-07 | 5.9 +3.6/−2.4 | 1.6 | 2.4e-10 | −0.1 +1.9/0.0 | −0.1 | 1.0 |
| 50 | 165343.0−015238 | 253.42925 | −1.87735 | 0.26 | 5.4 | 463 | −0.33 | 32.4 +6.8/−5.7 | 4.8 | 0.0 | 21.7 +5.8/−4.7 | 3.8 | 2.3e-32 | 10.6 +4.4/−3.3 | 2.4 | 9.4e-13 |
| 51 | 165343.4−015841 | 253.43123 | −1.97813 | 0.16 | 0.7 | 500 | −0.43 | 5.9 +3.6/−2.4 | 1.6 | 8.2e-11 | 6.0 +3.6/−2.4 | 1.7 | 1.3e-13 | 0.0 +1.9/0.0 | 0.0 | 1.0 |
| 52 | 165344.0−014945 | 253.43351 | −1.82921 | 1.23 | 8.3 | 355 | −0.21 | 7.0 +4.3/−3.1 | 1.6 | 1.5e-03 | 3.0 +3.2/−1.9 | 0.9 | 2.4e-02 | 4.0 +3.6/−2.4 | 1.1 | 1.9e-02 |
| 53 | 165344.1−020355 | 253.43404 | −2.06545 | 1.17 | 5.9 | 438 | ... | 2.3 +2.9/−1.6 | 0.8 | 3.5e-02 | −0.3 +1.9/0.0 | −0.2 | 1.0 | 2.6 +2.9/−1.6 | 0.9 | 8.4e-03 |
| 54 | 165344.4−015306 | 253.43509 | −1.88505 | 0.67 | 4.9 | 462 | −0.13 | 3.5 +3.2/−1.9 | 1.1 | 1.5e-03 | −0.2 +1.9/0.0 | −0.1 | 1.0 | 3.7 +3.2/−1.9 | 1.2 | 1.8e-04 |
| 55 | 165345.4−020434 | 253.43935 | −2.07631 | 1.12 | 6.6 | 445 | −0.40 | 3.8 +3.4/−2.2 | 1.1 | 7.9e-03 | −0.4 +1.9/0.0 | −0.2 | 1.0 | 4.3 +3.4/−2.2 | 1.2 | 1.2e-03 |
| 56 | 165345.5−020209 | 253.43993 | −2.03600 | 0.63 | 4.2 | 494 | ... | 2.7 +2.9/−1.6 | 0.9 | 5.1e-03 | 0.8 +2.3/−0.8 | 0.4 | 1.5e-01 | 1.8 +2.7/−1.3 | 0.7 | 1.5e-02 |
| 57 | 165346.0−020133 | 253.44181 | −2.02587 | 0.28 | 3.6 | 495 | −0.08 | 8.8 +4.1/−2.9 | 2.1 | 1.6e-12 | 6.9 +3.8/−2.6 | 1.8 | 3.9e-12 | 1.9 +2.7/−1.3 | 0.7 | 7.6e-03 |
| 58 | 165346.7−020109 | 253.44466 | −2.01930 | 0.21 | 3.2 | 501 | −0.03 | 11.8 +4.6/−3.4 | 2.6 | 2.7e-18 | 5.9 +3.6/−2.4 | 1.6 | 6.1e-11 | 5.9 +3.6/−2.4 | 1.6 | 4.8e-09 |
| 59 | 165347.0−015403 | 253.44594 | −1.90108 | 0.27 | 4.0 | 444 | −0.25 | 11.8 +4.6/−3.4 | 2.6 | 1.7e-16 | 10.9 +4.4/−3.3 | 2.5 | 7.7e-19 | 0.9 +2.3/−0.8 | 0.4 | 1.4e-01 |
| 60 | 165347.0−015054 | 253.44604 | −1.84837 | 0.43 | 7.2 | 437 | −0.07 | 35.2 +7.1/−6.1 | 4.9 | 8.9e-33 | 23.4 +6.0/−4.9 | 3.9 | 3.2e-27 | 11.8 +4.7/−3.6 | 2.5 | 1.7e-09 |
| 61 | 165347.7−020610 | 253.44878 | −2.10295 | 1.89 | 8.2 | 400 | −0.32 | 2.2 +3.4/−2.2 | 0.7 | 1.5e-01 | 4.0 +3.4/−2.2 | 1.2 | 5.4e-03 | −1.7 +1.9/0.0 | −0.9 | 1.0 |
| 62 | 165348.0−015400 | 253.45007 | −1.90003 | 0.15 | 4.1 | 347 | −0.09 | 42.8 +7.6/−6.5 | 5.6 | 0.0 | 19.9 +5.6/−4.4 | 3.6 | 0.0 | 22.9 +5.9/−4.8 | 3.9 | 0.0 |
| 63 | 165348.8−015413 | 253.45368 | −1.90380 | 0.50 | 4.0 | 435 | −0.30 | 3.8 +3.2/−1.9 | 1.2 | 1.3e-04 | 2.9 +2.9/−1.6 | 1.0 | 1.4e-04 | 0.8 +2.3/−0.8 | 0.4 | 1.4e-01 |
| 64 | 165349.4−015818 | 253.45593 | −1.97174 | 0.20 | 1.4 | 310 | −0.19 | 6.0 +3.6/−2.4 | 1.7 | 3.1e-11 | 1.0 +2.3/−0.8 | 0.4 | 1.1e-02 | 5.0 +3.4/−2.2 | 1.5 | 1.5e-09 |
| 65 | 165349.6−015414 | 253.45701 | −1.90397 | 0.60 | 4.0 | 476 | ... | 2.7 +2.9/−1.6 | 0.9 | 2.6e-03 | 1.9 +2.7/−1.3 | 0.7 | 5.5e-03 | 0.8 +2.3/−0.8 | 0.4 | 1.5e-01 |
| 66 | 165349.9−015242 | 253.45828 | −1.87845 | 0.89 | 5.5 | 309 | ... | 2.4 +2.9/−1.6 | 0.8 | 2.0e-02 | 1.7 +2.7/−1.3 | 0.7 | 3.0e-02 | 0.7 +2.3/−0.8 | 0.3 | 2.6e-01 |

**Table 6**
(Continued)

| *N* | CXOU J Name | R.A. (deg) | Decl. (deg) | *r* (″) | *D* (′) | $A_{\rm eff}$ ($\rm cm^2$) | log $P_{\rm K-S}$ | Counts (0.5–8 keV) | $\sigma$ | $P_{\rm B}$ | Counts (0.5–2 keV) | $\sigma$ | $P_{\rm B}$ | Counts (2–8 keV) | $\sigma$ | $P_{\rm B}$ |
|---|---|---|---|---|---|---|---|---|---|---|---|---|---|---|---|---|
| 67 | 165350.4−015508 | 253.46021 | −1.91900 | 0.15 | 3.3 | 456 | −0.40 | 26.9 +6.3/−5.2 | 4.3 | 0.0 | 8.0 +4.0/−2.8 | 2.0 | 6.7e-16 | 18.9 +5.4/−4.3 | 3.5 | 8.9e-37 |
| 68 | 165350.5−015825 | 253.46055 | −1.97379 | 0.30 | 1.7 | 301 | ... | 3.0 +2.9/−1.6 | 1.0 | 1.6e-05 | 0.0 +1.9/0.0 | 0.0 | 1.0 | 3.0 +2.9/−1.6 | 1.0 | 3.9e-06 |
| 69 | 165351.9−015847 | 253.46666 | −1.97973 | 0.20 | 2.2 | 214 | −0.17 | 7.0 +3.8/−2.6 | 1.8 | 4.7e-14 | 3.0 +2.9/−1.6 | 1.0 | 1.2e-06 | 4.0 +3.2/−1.9 | 1.2 | 1.2e-08 |
| 70 | 165356.0−020251 | 253.48362 | −2.04764 | 0.37 | 5.7 | 477 | −1.68 | 21.0 +5.8/−4.7 | 3.6 | 4.2e-21 | 12.6 +4.7/−3.6 | 2.7 | 4.2e-15 | 8.4 +4.1/−2.9 | 2.0 | 4.2e-08 |
| 71 | 165357.4−015239 | 253.48957 | −1.87760 | 0.56 | 6.4 | 447 | −0.15 | 14.5 +5.1/−4.0 | 2.8 | 2.4e-11 | 6.4 +3.8/−2.6 | 1.7 | 5.0e-06 | 8.1 +4.1/−2.9 | 2.0 | 1.1e-06 |
| 72 | 165357.6−015740 | 253.49014 | −1.96121 | 0.27 | 3.5 | 487 | −0.10 | 8.8 +4.1/−2.9 | 2.1 | 5.4e-13 | 6.9 +3.8/−2.6 | 1.8 | 4.5e-12 | 1.9 +2.7/−1.3 | 0.7 | 4.9e-03 |
| 73 | 165358.4−015526 | 253.49364 | −1.92406 | 0.60 | 4.5 | 481 | −0.10 | 3.6 +3.2/−1.9 | 1.1 | 6.4e-04 | −0.1 +1.9/0.0 | −0.1 | 1.0 | 3.8 +3.2/−1.9 | 1.2 | 1.2e-04 |
| 74 | 165358.6−020018 | 253.49433 | −2.00525 | 0.69 | 4.4 | 342 | ... | 2.7 +2.9/−1.6 | 0.9 | 3.3e-03 | 0.9 +2.3/−0.8 | 0.4 | 9.8e-02 | 1.8 +2.7/−1.3 | 0.7 | 1.6e-02 |
| 75 | 165359.0−020316 | 253.49594 | −2.05447 | 0.12 | 6.5 | 385 | −0.08 | 312.5 +18.7/−17.7 | 16.7 | 0.0 | 170.4 +14.1/−13.1 | 12.1 | 0.0 | 142.1 +13.0/−11.9 | 10.9 | 0.0 |
| 76 | 165359.3−015630 | 253.49718 | −1.94175 | 0.60 | 4.2 | 451 | ... | 2.7 +2.9/−1.6 | 0.9 | 3.1e-03 | 1.9 +2.7/−1.3 | 0.7 | 5.2e-03 | 0.8 +2.3/−0.8 | 0.3 | 1.6e-01 |
| 77 | 165400.4−015454 | 253.50192 | −1.91503 | 0.90 | 5.2 | 469 | ... | 2.5 +2.9/−1.6 | 0.8 | 1.9e-02 | −0.2 +1.9/0.0 | −0.1 | 1.0 | 2.7 +2.9/−1.6 | 0.9 | 4.8e-03 |
| 78 | 165400.5−015826 | 253.50237 | −1.97406 | 0.67 | 4.2 | 448 | ... | 2.6 +2.9/−1.6 | 0.9 | 7.9e-03 | 1.9 +2.7/−1.3 | 0.7 | 1.0e-02 | 0.8 +2.3/−0.8 | 0.3 | 2.2e-01 |
| 79 | 165400.8−015549 | 253.50362 | −1.93053 | 0.77 | 4.8 | 476 | ... | 2.6 +2.9/−1.6 | 0.9 | 1.0e-02 | −0.2 +1.9/0.0 | −0.1 | 1.0 | 2.7 +2.9/−1.6 | 0.9 | 2.6e-03 |
| 80 | 165401.1−020048 | 253.50496 | −2.01335 | 0.31 | 5.2 | 432 | −1.11 | 24.3 +6.1/−5.0 | 4.0 | 1.4e-29 | 21.7 +5.8/−4.7 | 3.8 | 1.3e-32 | 2.6 +2.9/−1.6 | 0.9 | 8.5e-03 |
| 81 | 165401.5−015053 | 253.50641 | −1.84824 | 1.19 | 8.4 | 338 | −1.82 | 9.1 +4.6/−3.4 | 2.0 | 8.3e-05 | 4.1 +3.4/−2.2 | 1.2 | 3.4e-03 | 5.0 +3.8/−2.6 | 1.3 | 5.5e-03 |
| 82 | 165402.0−015854 | 253.50846 | −1.98171 | 0.43 | 4.6 | 439 | −0.02 | 8.6 +4.1/−2.9 | 2.1 | 5.1e-10 | 4.9 +3.4/−2.2 | 1.4 | 4.7e-07 | 3.8 +3.2/−1.9 | 1.2 | 1.5e-04 |
| 83 | 165402.1−015322 | 253.50909 | −1.88970 | 1.12 | 6.5 | 455 | −0.28 | 3.6 +3.4/−2.2 | 1.1 | 1.7e-02 | 4.4 +3.4/−2.2 | 1.3 | 4.5e-04 | −0.9 +1.9/0.0 | −0.5 | 1.0 |
| 84 | 165402.9−015425 | 253.51220 | −1.90706 | 0.69 | 6.0 | 461 | −0.16 | 7.0 +4.0/−2.8 | 1.8 | 9.6e-06 | 4.6 +3.4/−2.2 | 1.4 | 5.4e-05 | 2.4 +2.9/−1.6 | 0.8 | 2.4e-02 |
| 85 | 165404.5−020346 | 253.51891 | −2.06305 | 0.59 | 7.7 | 423 | −0.49 | 26.0 +6.5/−5.4 | 4.0 | 1.1e-17 | 18.9 +5.6/−4.4 | 3.4 | 8.6e-17 | 7.1 +4.1/−2.9 | 1.7 | 2.5e-04 |
| 86 | 165405.6−015905 | 253.52360 | −1.98490 | 0.60 | 5.6 | 473 | −0.13 | 9.1 +4.3/−3.1 | 2.1 | 4.7e-08 | −0.3 +1.9/0.0 | −0.2 | 1.0 | 9.4 +4.3/−3.1 | 2.2 | 9.1e-10 |
| 87 | 165406.9−020540 | 253.52901 | −2.09457 | 0.90 | 9.6 | 423 | −0.12 | 22.9 +6.5/−5.4 | 3.5 | 6.9e-11 | 12.5 +5.0/−3.8 | 2.5 | 2.3e-07 | 10.5 +4.9/−3.7 | 2.2 | 3.6e-05 |
| 88 | 165407.3−015957 | 253.53044 | −1.99918 | 1.19 | 6.2 | 463 | −0.35 | 2.8 +3.2/−1.9 | 0.9 | 3.9e-02 | 3.5 +3.2/−1.9 | 1.1 | 2.0e-03 | −0.7 +1.9/0.0 | −0.4 | 1.0 |
| 89 | 165409.8−020219 | 253.54089 | −2.03870 | 0.54 | 7.8 | 445 | −0.16 | 32.0 +7.0/−5.9 | 4.6 | 7.5e-24 | 18.8 +5.6/−4.4 | 3.4 | 9.2e-17 | 13.2 +5.0/−3.8 | 2.7 | 2.6e-09 |
| 90 | 165409.9−015736 | 253.54128 | −1.96018 | 1.44 | 6.5 | 456 | −0.55 | 2.8 +3.2/−1.9 | 0.9 | 3.3e-02 | 3.6 +3.2/−1.9 | 1.1 | 1.0e-03 | −0.8 +1.9/0.0 | −0.4 | 1.0 |
| 91 | 165411.9−015610 | 253.54964 | −1.93620 | 0.72 | 7.3 | 450 | −0.03 | 12.8 +5.0/−3.8 | 2.6 | 2.7e-08 | 10.2 +4.4/−3.3 | 2.3 | 3.5e-09 | 2.6 +3.2/−1.9 | 0.8 | 5.7e-02 |
| 92 | 165412.6−015701 | 253.55287 | −1.95052 | 0.81 | 7.3 | 452 | −1.72 | 10.1 +4.6/−3.4 | 2.2 | 1.7e-06 | 4.4 +3.4/−2.2 | 1.3 | 6.5e-04 | 5.7 +3.8/−2.6 | 1.5 | 5.7e-04 |
| 93 | 165414.5−015707 | 253.56049 | −1.95214 | 1.38 | 7.7 | 395 | −0.10 | 4.9 +3.8/−2.6 | 1.3 | 6.5e-03 | −0.6 +1.9/0.0 | −0.3 | 1.0 | 5.5 +3.8/−2.6 | 1.4 | 1.2e-03 |
| 94 | 165414.8−015442 | 253.56181 | −1.91192 | 0.69 | 8.4 | 435 | −0.33 | 24.7 +6.4/−5.3 | 3.9 | 6.5e-16 | 16.0 +5.2/−4.1 | 3.1 | 1.9e-14 | 8.6 +4.4/−3.3 | 1.9 | 6.0e-05 |
| 95 | 165415.3−015455 | 253.56394 | −1.91547 | 1.79 | 8.5 | 435 | −0.25 | 2.4 +3.6/−2.4 | 0.7 | 1.7e-01 | 2.7 +3.2/−1.9 | 0.8 | 4.8e-02 | −0.3 +2.7/−1.3 | −0.1 | 6.8e-01 |
| 96 | 165416.8−015749 | 253.57027 | −1.96382 | 1.45 | 8.3 | 437 | −0.09 | 4.6 +4.0/−2.8 | 1.2 | 2.6e-02 | 5.0 +3.6/−2.4 | 1.4 | 1.1e-03 | −0.4 +2.7/−1.3 | −0.1 | 6.9e-01 |
| 97 | 165418.2−020018 | 253.57588 | −2.00523 | 1.30 | 8.9 | 363 | −0.54 | 7.7 +4.6/−3.4 | 1.7 | 2.0e-03 | 6.3 +4.0/−2.8 | 1.6 | 5.3e-04 | 1.4 +3.2/−1.9 | 0.4 | 2.7e-01 |

**Table 7**
Potential Counterpart Matches to the *Chandra* X-Ray Sources from the USNO B1.0 Catalog

| *N* | USNO B1.0 Name | Offset | *B*2 | *R*2 | *I* | USNO B1.0 Position | |
|---|---|---|---|---|---|---|---|
| | | (″) | (mag) | (mag) | (mag) | R.A. | Decl. |
| | | | 0FGL J1311.9−3419 | | | | |
| 20 | 0555−0290744 | 1.06 | 16.07 | 14.89 | 14.32 | 13 11 34.425 | −34 29 20.44 |
| 31 | 0555−0290806 | 0.37 | 19.67 | 18.87 | 18.33 | 13 11 43.735 | −34 27 49.78 |
| 35 | 0554−0289419 | 0.62 | 21.02 | ... | ... | 13 11 45.741 | −34 30 29.96 |
| 43 | 0553−0287487 | 0.58 | 20.09 | 20.03 | ... | 13 11 49.204 | −34 38 17.31 |
| 45 | 0554−0289445 | 1.67 | 17.53 | 15.65 | 14.92 | 13 11 49.518 | −34 33 31.73 |
| 54 | 0555−0290875 | 0.25 | 18.03 | 16.90 | 16.72 | 13 11 54.978 | −34 26 42.54 |
| 61 | 0555−0290895 | 0.62 | 20.88 | 19.97 | ... | 13 11 58.216 | −34 27 33.73 |
| ... | 0555−0290894 | 1.36 | ... | 19.15 | 18.49 | 13 11 58.165 | −34 27 34.77 |
| 64 | 0554−0289501 | 0.66 | 20.80 | 19.89 | ... | 13 11 59.537 | −34 35 54.96 |
| 66 | 0554−0289512 | 0.74 | 16.63 | 15.50 | 14.22 | 13 12 02.102 | −34 32 34.62 |
| 69 | 0556−0290675 | 2.30 | 16.67 | 14.48 | 13.05 | 13 12 04.097 | −34 20 26.25 |
| 75 | 0554−0289533 | 0.34 | 21.00 | 20.39 | ... | 13 12 06.126 | −34 31 52.63 |
| 78 | 0554−0289544 | 0.22 | 21.19 | ... | ... | 13 12 07.411 | −34 31 07.71 |
| 82 | 0554−0289558 | 1.81 | 18.75 | 18.15 | 17.53 | 13 12 09.823 | −34 34 38.80 |
| 85 | 0555−0290992 | 0.95 | 21.08 | ... | 18.69 | 13 12 18.364 | −34 28 19.28 |
| 89 | 0555−0291020 | 0.88 | 18.97 | 18.69 | 17.82 | 13 12 23.109 | −34 29 12.04 |
| 91 | 0555−0291038 | 0.20 | 13.11 | 11.87 | 11.38 | 13 12 25.362 | −34 25 01.51 |
| 96 | 0555−0291083 | 1.02 | 20.48 | 19.88 | ... | 13 12 34.909 | −34 29 25.27 |
| | | | 0FGL J1653.4−0200 | | | | |
| 8 | 0880−0368721 | 0.50 | 18.47 | 16.97 | 16.96 | 16 53 15.616 | −01 58 22.66 |
| ... | 0880−0368718 | 1.85 | ... | 18.01 | 19.27 | 16 53 15.537 | −01 58 23.75 |
| 23 | 0881−0336447 | 2.75 | 20.59 | 19.45 | 20.06 | 16 53 27.505 | −01 51 15.69 |
| 25 | 0880−0368904 | 1.62 | ... | 19.89 | ... | 16 53 29.935 | −01 58 28.39 |
| ... | 0880−0368902 | 1.67 | 20.47 | 19.28 | 18.13 | 16 53 29.928 | −01 58 27.65 |
| 28 | 0881−0336518 | 0.79 | 10.78 | 9.56 | 9.05 | 16 53 33.598 | −01 52 59.72 |
| 30 | 0879−0416563 | 1.77 | ... | 20.39 | 19.33 | 16 53 34.735 | −02 00 31.96 |
| ... | 0879−0416560 | 2.95 | ... | 19.43 | 19.10 | 16 53 34.686 | −02 00 30.07 |
| 36 | 0879−0416588 | 0.53 | 19.72 | 17.93 | 18.01 | 16 53 37.207 | −02 04 42.56 |
| 38 | 0880−0369025 | 0.28 | 20.40 | 19.41 | 20.0 | 16 53 38.070 | −01 58 36.71 |
| 40 | 0880−0369044 | 0.58 | 20.64 | 19.42 | 18.54 | 16 53 39.115 | −01 54 12.08 |
| 44 | 0880−0369077 | 0.68 | 20.58 | 18.95 | 17.05 | 16 53 41.410 | −01 59 27.68 |
| ... | 0880−0369078 | 2.36 | 20.89 | 19.29 | ... | 16 53 41.438 | −01 59 29.31 |
| 49 | 0879−0416658 | 0.32 | 16.64 | 14.60 | 14.16 | 16 53 42.849 | −02 01 45.09 |
| 59 | 0880−0369161 | 0.73 | 19.05 | 16.05 | 15.06 | 16 53 47.071 | −01 54 04.14 |
| 60 | 0881−0336669 | 0.37 | 20.35 | 19.38 | ... | 16 53 47.030 | −01 50 54.32 |
| 61 | 0878−0449662 ··· | 2.87 | ... | 19.44 | 19.44 | 16 53 47.630 | −02 06 13.25 |
| 75 | 0879−0416898 | 2.27 | 18.75 | 17.31 | 16.49 | 16 53 59.085 | −02 03 13.99 |
| 80 | 0879−0416929 | 0.72 | 20.58 | 18.62 | 17.01 | 16 54 01.230 | −02 00 48.46 |
| 97 | 0879−0417221 | 0.54 | 13.94 | 12.27 | 12.02 | 16 54 18.222 | −02 00 19.33 |

*Fermi*-LAT source, 0FGL J2339.8−0530 (Kong et al. 2012). Another bright X-ray source, CXOU J131147.0−343205, found just outside the LAT error ellipse and also previously detected by *Suzaku*, did not show any significant X-ray variability, and is a less probable counterpart to the $\gamma$-ray source.

In the case of 0FGL J1653.4−0200, the brightest X-ray source (CXOU J165338.0−015836) within the *Fermi*-LAT localization also displays a nonthermal X-ray spectrum from our *Chandra* observation. However, there was no significant X-ray variability found within our 20 ks observation, and on the longer timescale probed by comparing to a *Swift* observation obtained ∼10 months earlier. A faint optical counterpart to this X-ray source is found, and optical photometric and spectroscopic monitoring may be fruitful to test whether this source is similar to the case of CXOU J233938.7−053305. The second brightest *Chandra* source (CXOU J165341.4−015927) found within the 2FGL localization also has an optical/infrared counterpart, and has a likely thermal origin for the X-rays. This, and the other fainter X-ray sources revealed in our *Chandra* observation, can be similarly investigated to ultimately probe the nature of this unidentified $\gamma$-ray source.

We thank S. Digel, M. Wolff, E. Hays, and Ł. Stawarz for comments on the manuscript, T. Burnett, E. Ferrara, E. Hays, Y. Kanai, J. Kataoka, N. Kawai, M. Kerr, T. Nakamori, P. Ray, D. J. Thompson, N. Vilchez, and M. T. Wolff for their support and participation in the *Chandra* observing proposal, and members of the *Fermi*-LAT team for providing the preliminary LAT localizations utilized over the course of this work.

This work began while C.C.C. was supported by an appointment to the NASA Postdoctoral Program at Goddard Space Flight Center, administered by Oak Ridge Associated Universities through a contract with NASA; his work at NRL is supported in part by NASA DPR S-15633-Y. Support for this work

**Table 8**
Potential Counterpart Matches to the *Chandra* X-Ray Sources in the 2MASS Catalog

| *N* | 2MASS Name | Offset (″) | *J* (Error) (mag) | *H* (Error) (mag) | *K* (Error) (mag) |
|---|---|---|---|---|---|
| | | 0FGL J1311.9−3419 | | | |
| 20 | J13113441−3429208 | 0.64 | 14.324 (0.027) | 14.038 (0.038) | 13.998 (0.045) |
| 45 | J13114950−3433318 | 1.93 | 14.449 (0.032) | 13.934 (0.027) | 13.834 (0.037) |
| 54 | J13115497−3426426 | 0.16 | 16.099 (0.100) | 15.444 (0.086) | 14.999 (0.124) |
| 66 | J13120210−3432341 | 0.61 | 14.588 ( ⋯ ) | 14.629 (0.080) | 13.613 ( ⋯ ) |
| 69 | J13120408−3420263 | 2.19 | 12.636 (0.026) | 11.960 (0.025) | 11.825 (0.023) |
| 91 | J13122539−3425015 | 0.42 | 11.294 (0.023) | 10.971 (0.023) | 10.892 (0.023) |
| | | 0FGL J1653.4−0200 | | | |
| 8 | J16531562−0158224 | 0.35 | 16.196 (0.127) | 15.560 (0.147) | 14.292 (0.088) |
| 28 | J16533360−0152597 | 0.89 | 8.522 (0.020) | 8.067 (0.020) | 7.996 (0.023) |
| 44 | J16534140−0159272 | 0.27 | 15.094 (0.056) | 14.469 (0.059) | 14.147 (0.066) |
| 49 | J16534285−0201450 | 0.31 | 13.133 (0.023) | 12.575 (0.026) | 12.492 (0.030) |
| 59 | J16534707−0154041 | 0.73 | 13.634 (0.033) | 12.942 (0.034) | 12.737 (0.036) |
| 75 | J16535902−0203163 | 0.30 | 16.488 (0.195) | 15.624 (0.153) | 14.575 (0.112) |
| 80 | J16540121−0200480 | 0.31 | 15.007 (0.057) | 14.380 (0.055) | 14.043 (0.076) |
| 97 | J16541823−0200193 | 0.59 | 11.079 (0.021) | 10.696 (0.023) | 10.539 (0.022) |

was partially provided by the National Aeronautics and Space Administration through *Chandra* Award Number GO0-11022A (C.C.C. and D.D.) issued by the Chandra X-ray Observatory Center, which is operated by the Smithsonian Astrophysical Observatory for and on behalf of the National Aeronautics Space Administration under contract NAS8-03060.

*Facilities: CXO*, *Swift*

## APPENDIX A

## X-RAY SOURCE LISTS

This section lists the X-ray properties of all sources detected in the four ACIS-I chips of the *Chandra* fields (see Section 2.1). In Table 5 (0FGL J1311.9−3419) and Table 6 (0FGL J1653.4−0200), sources are listed with their catalog numbers (*N*) in order of increasing R.A. with coordinates in J2000.0. Listed also are the source localization errors (*r*), its distance from the *Chandra* aim point (*D*), the effective area ($A_{\rm eff}$) at the source position at 1.5 keV (lower values indicate sources located closer to the chip gaps and edges), the logarithm probability from the KS test for variability (log $P_{\rm K-S}$), and the net counts, significances ($\sigma$), and probability ($P_{\rm B}$) that the source counts are solely from the background in the 0.5–8 keV, 0.5–2 keV, and 2–8 keV bands. Following Broos et al. (2010), we considered only sources with more than four net counts in the full band and not near the CCD chip edges, and found five sources in each of the ACIS-I fields to be possibly variable ($0.005 < P_{\rm K-S} < 0.05$)—0FGL J1311.9−3419 (N34, N49, N76, N88, and N89) and 0FGL J1653.4−0200 (N14, N37, N70, N81, and N92). There is no evidence for variability ($P_{\rm K-S} > 0.05$) in the remaining sources. The analysis described in Section 2.1 also provides an afterglow fraction, which, if >0, indicates that the source is possibly contaminated by afterglow events and their significance could be lower than quoted and the source position, spectrum, and/or light curve are potentially affected. The sources flagged in this way were J131145.71−343030.5 (N35), J131147.03−343205.2 (N39), J131226.81−343029.7 (N93), J165315.60−015822.1 (N8), J165323.22−020451.2 (N14), J165325.88−015107.7 (N19), J165333.54−015259.5 (N28), J165338.05−015836.6 (N38), and J165359.02−020316.0 (N75).

## APPENDIX B

## OPTICAL, NEAR-INFRARED, AND MID-INFRARED COUNTERPARTS

We cross-matched the *Chandra* X-ray source lists (Appendix A) for 0FGL J1311.9−3419 and 0FGL J1653.4−0200 with the USNO B1.0 optical, 2MASS near-infrared, and WISEP mid-infrared catalogs. The *WISE* bands are in the 3.4 ($W1$), 4.6 ($W2$), 12 ($W3$), and 22 $\mu$m ($W4$) bandpasses. In order to include as many potential matches as practical, we used a relatively liberal search radius of 3″ from the *Chandra* positions, although a comparison of the *Chandra* images with the optical/IR ones shows the most believable counterparts have <1″–2″ offsets. Out of the 97 sources found in each of the *Chandra* fields, we located potential USNO B1.0 counterparts for up to 17 (one with two optical matches) and 16 (four with two optical matches) X-ray sources in the 0FGL J1311.9−3419 and 0FGL J1653.4−0200 fields, respectively (Table 7). In the 2MASS catalog, we found up to six and eight matches for these respective fields (Table 8). In the WISEP catalog, there were up to 25 and 21 matches, respectively (Table 9). All 2MASS matches were also found in the USNO B1.0 and WISEP catalogs. In the 0FGL J1311.9−3419 and 0FGL J1653.4−0200 fields, seven and three WISEP sources respectively, had USNO B1.0 counterparts but no 2MASS ones. There were 12 and 10 WISEP matches with X-ray sources without matches in the USNO B1.0 and 2MASS catalogs in the two respective fields.

To quantify possible systematic errors in the *Chandra* positions, we calculated the differences, $\delta$(R.A., decl.) = (R.A., decl.)$_{\rm USNO}$ − (R.A., decl.)$_{\textit{Chandra}}$, for all X-ray sources with $\gtrsim$4 net counts and detected at >1.0$\sigma$ that are within 1″ of a USNO source. For 11 sources in the 0FGL J1311.9−3419 and 10 sources in the 0FGL J1653.4−0200 fields, we found average offsets, $\delta$(R.A., decl.) = (−0.″06 ± 0.″44, −0.″08 ± 0.″44) and (0.″36 ± 0.″34, 0.″37 ± 0.″18), respectively. Thus, only the X-ray

**Table 9**
Potential Counterpart Matches to the *Chandra* X-ray Sources in the WISEP Catalog

| *N* | WISEP Name | Offset (″) | *W*1 (Error) (mag) | *W*2 (Error) (mag) | *W*3 (Error) (mag) | *W*4 (Error) (mag) |
|---|---|---|---|---|---|---|
| | | | 0FGL J1311.9−3419 | | | |
| 13 | J131129.38−343134.0 | 0.77 | 16.899 (0.150) | 15.992 (0.232) | 12.732 ( · · · ) | 8.665 ( · · · ) |
| 20 | J131134.41−342920.6 | 0.78 | 13.853 (0.031) | 13.840 (0.047) | 12.449 ( · · · ) | 8.534 ( · · · ) |
| 29 | J131142.16−342955.8 | 2.56 | 16.397 (0.101) | 16.042 (0.233) | 12.343 ( · · · ) | 9.180 ( · · · ) |
| 31 | J131143.72−342749.9 | 0.18 | 15.790 (0.067) | 15.302 (0.128) | 11.432 (0.169) | 7.954 (0.193) |
| 32 | J131143.98−342500.4 | 0.28 | 15.518 (0.057) | 15.039 (0.111) | 12.290 (0.364) | 9.219 ( · · · ) |
| 34 | J131145.72−343312.4 | 1.50 | 16.197 (0.080) | 15.527 (0.150) | 12.766 ( · · · ) | 9.008 ( · · · ) |
| 39 | J131147.09−343205.3 | 0.69 | 15.720 (0.063) | 14.949 (0.095) | 12.226 (0.333) | 9.056 (0.463) |
| 40 | J131147.15−342953.5 | 1.25 | 16.846 (0.152) | 16.408 (0.345) | 12.443 ( · · · ) | 8.721 ( · · · ) |
| 43 | J131149.24−343817.3 | 0.30 | 16.639 (0.135) | 15.609 (0.177) | 12.457 (0.450) | 8.850 ( · · · ) |
| 45 | J131149.51−343331.4 | 1.57 | 13.762 (0.030) | 13.750 (0.043) | 12.498 ( · · · ) | 9.219 ( · · · ) |
| 54 | J131154.98−342642.1 | 0.63 | 14.474 (0.034) | 14.207 (0.060) | 12.009 ( · · · ) | 8.806 ( · · · ) |
| 55 | J131156.02−342124.8 | 2.32 | 16.738 (0.149) | 16.522 (0.405) | 12.550 ( · · · ) | 8.838 ( · · · ) |
| 64 | J131159.49−343553.6 | 2.03 | 16.539 (0.115) | 15.237 (0.121) | 12.548 (0.448) | 8.655 ( · · · ) |
| 65 | J131200.45−343231.4 | 0.56 | 16.542 (0.115) | 15.604 (0.168) | 12.172 ( · · · ) | 9.120 ( · · · ) |
| 66 | J131202.10−343235.1 | 1.19 | 13.230 (0.027) | 13.058 (0.033) | 10.312 (0.069) | 7.975 (0.197) |
| 69 | J131204.09−342026.3 | 2.27 | 11.709 (0.025) | 11.669 (0.023) | 11.842 (0.234) | 9.138 ( · · · ) |
| 70 | J131203.88−343652.3 | 1.11 | 17.032 (0.187) | 15.248 (0.125) | 12.540 (0.480) | 9.006 ( · · · ) |
| 75 | J131206.11−343151.3 | 1.15 | 16.081 (0.107) | 15.533 (0.173) | 12.090 ( · · · ) | 8.641 ( · · · ) |
| 76 | J131206.16−343446.8 | 2.86 | 13.466 (0.027) | 13.034 (0.034) | 11.171 (0.134) | 8.687 (0.379) |
| 77 | J131206.59−342909.6 | 0.76 | 16.366 (0.109) | 16.211 (0.303) | 12.652 ( · · · ) | 8.773h ( · · · ) |
| 78 | J131207.47−343107.8 | 0.89 | 16.417 (0.112) | 16.119 (0.291) | 12.307 ( · · · ) | 8.833 ( · · · ) |
| 82 | J131209.82−343438.9 | 1.67 | 15.317 (0.050) | 15.059 (0.106) | 12.203 ( · · · ) | 8.669 (0.336) |
| 87 | J131220.24−342930.7 | 0.94 | 16.492 (0.122) | 16.160 (0.281) | 12.384 (0.416) | 8.948 ( · · · ) |
| 89 | J131223.15−342912.2 | 0.57 | 15.169 (0.049) | 14.785 (0.087) | 11.711 (0.228) | 8.504 ( · · · ) |
| 91 | J131225.40−342501.5 | 0.50 | 10.817 (0.024) | 10.806 (0.022) | 10.612 (0.086) | 8.546 ( · · · ) |
| | | | 0FGL J1653.4−0200 | | | |
| 2 | J165307.76−015955.5 | 1.46 | 15.841 (0.069) | 14.383 (0.066) | 11.470 (0.180) | 8.545 (0.373) |
| 3 | J165309.03−020139.0 | 0.70 | 15.791 (0.064) | 15.597 (0.163) | 12.478 ( · · · ) | 9.131 ( · · · ) |
| 4 | J165309.82−015915.2 | 1.70 | 15.608 (0.060) | 15.257 (0.128) | 12.032 ( · · · ) | 9.141 ( · · · ) |
| 7 | J165315.14−020314.2 | 1.48 | 16.552 (0.113) | 16.642 (0.403) | 12.076 ( · · · ) | 8.810 ( · · · ) |
| 8 | J165315.62−015822.3 | 0.41 | 12.599 (0.025) | 11.578 (0.025) | 9.208 (0.037) | 7.364 (0.113) |
| 11 | J165318.45−015432.3 | 2.45 | 16.885 (0.154) | 16.508 (0.376) | 12.306 (0.388) | 8.957 ( · · · ) |
| 14 | J165323.24−020451.1 | 0.34 | 16.240 (0.089) | 15.220 (0.121) | 12.150 ( · · · ) | 9.074 ( · · · ) |
| 25 | J165329.94−015826.7 | 1.78 | 15.589 (0.057) | 15.529 (0.159) | 12.340 ( · · · ) | 9.112 ( · · · ) |
| 28 | J165333.57−015259.6 | 0.38 | 7.934 (0.021) | 7.990 (0.023) | 7.915 (0.023) | 7.926 (0.198) |
| 36 | J165337.19−020442.5 | 0.41 | 16.385 (0.093) | 16.687 (0.417) | 12.783 ( · · · ) | 9.083 ( · · · ) |
| 44 | J165341.41−015927.6 | 0.65 | 14.057 (0.031) | 13.843 (0.046) | 12.569 ( · · · ) | 8.667 ( · · · ) |
| 49 | J165342.83−020145.1 | 0.25 | 12.420 (0.026) | 12.429 (0.027) | 12.292 (0.413) | 9.014 ( · · · ) |
| 51 | J165343.52−015840.6 | 0.69 | 16.245 (0.100) | 16.366 (0.352) | 12.612 ( · · · ) | 8.882 ( · · · ) |
| 59 | J165347.05−015404.4 | 0.77 | 12.649 (0.025) | 12.584 (0.029) | 12.148 ( · · · ) | 8.501 ( · · · ) |
| 60 | J165347.06−015053.8 | 0.35 | 17.021 (0.174) | 15.530 (0.153) | 12.586 (0.493) | 8.923 ( · · · ) |
| 67 | J165350.45−015509.2 | 0.86 | 15.655 (0.066) | 14.910 (0.098) | 12.186 (0.365) | 8.562 ( · · · ) |
| 75 | J165359.08−020313.9 | 2.29 | 12.765 (0.025) | 12.142 (0.025) | 9.840 (0.050) | 7.213 (0.095) |
| 80 | J165401.19−020048.3 | 0.34 | 14.007 (0.030) | 13.776 (0.045) | 11.992 ( · · · ) | 9.009 ( · · · ) |
| 86 | J165405.67−015905.1 | 0.57 | 15.748 (0.061) | 14.702 (0.083) | 11.254 (0.155) | 8.766 (0.431) |
| 87 | J165406.91−020540.1 | 0.73 | 17.036 (0.182) | 15.394 (0.140) | 11.672 (0.208) | 8.533 ( · · · ) |
| 97 | J165418.21−020019.3 | 0.49 | 10.490 (0.023) | 10.515 (0.021) | 10.583 (0.088) | 8.850 ( · · · ) |

**Notes.** A single source is flagged with an "h" in the *W*4 band (J131206.59−342909.6, N77) as being possibly spurious or with photometry contaminated by scattered light from a nearby bright source.

positions in the 0FGL J1653.4−0200 field appear to have a significant systematic offset amounting to $r_{\rm syst.} = 0\farcs52 \pm 0\farcs39$.

## REFERENCES


Abdo, A. A., Ackermann, M., Ajello, M., et al. (*Fermi*-LAT Collaboration) 2009a, ApJS, 183, 46 (LAT Bright Source List)

Abdo, A. A., Ackermann, M., Ajello, M., et al. (*Fermi*-LAT Collaboration) 2009b, ApJ, 700, 597 (LAT Bright AGN Sample)

Abdo, A. A., Ackermann, M., Ajello, M., et al. (*Fermi*-LAT Collaboration) 2010a, ApJS, 188, 405 (1FGL Catalog)

Abdo, A. A., Ackermann, M., Ajello, M., et al. (*Fermi*-LAT Collaboration) 2010b, ApJ, 712, 1209 (PSR J1836+5925)

Abdo, A. A., Ackermann, M., Ajello, M., et al. (*Fermi*-LAT Collaboration) 2010c, ApJS, 187, 460 (1st Pulsar Catalog)

Abdo, A. A., Ackermann, M., Ajello, M., et al. (*Fermi*-LAT Collaboration) 2010d, ApJ, 710, 1271 (LBAS Spectra)

Abdo, A. A., Ackermann, M., Ajello, M., et al. (*Fermi*-LAT Collaboration) 2010e, Science, 328, 725 (Cen A Lobes)

Ackermann, M., Ajello, M., Allafort, A., et al. (*Fermi*-LAT Collaboration) 2011a, ApJ, 743, 171 (2nd LAT AGN Catalog)

Ackermann, M., Ajello, M., Allafort, A., et al. (*Fermi*-LAT Collaboration) 2011b, ApJ, 741, 30 (Radio/$\gamma$-ray AGN)

Ackermann, M., Ajello, M., Allafort, A., et al. (*Fermi*-LAT Collaboration) 2012, ApJ, 747, 104 (LAT Seyferts)
Atwood, W. B., Abdo, A. A., Ackermann, M., et al. (*Fermi*-LAT Collaboration) 2009, ApJ, 697, 1071
Broos, P. S., Townsley, L. K., Feigelson, E. D., et al. 2010, ApJ, 714, 1582
Burrows, D. N., Hill, J. E., Nousek, J. A., et al. 2005, Space Sci. Rev., 120, 165
Canosa, C. M., Worrall, D. M., Hardcastle, M. J., & Birkinshaw, M. 1999, MNRAS, 310, 30
Casandjian, J.-M., & Grenier, I. A. 2008, A&A, 489, 849
Cheung, C. C. 2007, in AIP Conf. Proc. 921, The First GLAST Symposium, ed. S. Ritz, P. Michelson, & C. A. Meegan (Melville, NY: AIP), 325
Cognard, I., Guillemot, L., Johnson, T. J., et al. 2011, ApJ, 732, 47
Condon, J. J., Cotton, W. D., Greisen, E. W., et al. 1998, AJ, 115, 1693
Crawford, F., Roberts, M. S. E., Hessels, J. W. T., et al. 2006, ApJ, 652, 1499
Cutri, R. M., Wright, E. L., Conrow, T., et al. 2012, VizieR Online Data Catalog, 2307, 0
Falcone, A., Stroh, M., Ferrara, E., et al. 2011, AAS/High Energy Astrophysics Division, 12, 04.03
Fruscione, A., McDowell, J. C., Allen, G. E., et al. 2006, Proc. SPIE, 6270, 60
Gehrels, N., Chincarini, G., Giommi, P., et al. 2004, ApJ, 611, 1005
Halpern, J. P., Gotthelf, E. V., Mirabal, N., & Camilo, F. 2002, ApJ, 573, L41
Hartman, R. C., Bertsch, D. L., Bloom, S. D., et al. 1999, ApJS, 123, 79
Kalberla, P. M. W., Burton, W. B., Hartmann, D., et al. 2005, A&A, 440, 775
Keith, M., Johnston, S., Ray, P. S., et al. 2011, MNRAS, 414, 1292
Kong, A. K. H., Huang, R. H. H., Cheng, K. S., et al. 2012, ApJ, 747, L3
La Palombara, N., Mignani, R. P., Hatziminaoglou, E., et al. 2006, A&A, 458, 245
Lenain, J.-P., Ricci, C., Türler, M., Dorner, D., & Walter, R. 2010, A&A, 524, A72
Maeda, K., Kataoka, J., Nakamori, T., et al. 2011, ApJ, 729, 103
Marelli, M., De Luca, A., & Caraveo, P. A. 2011, ApJ, 733, 82
McConville, W., Ostorero, L., Moderski, R., et al. 2011, ApJ, 738, 148
Mirabal, N., Halpern, J. P., Eracleous, M., & Becker, R. H. 2000, ApJ, 541, 180
Monet, D. G., Levine, S. E., Canzian, B., et al. 2003, AJ, 125, 984
Mukherjee, R., & Halpern, J. 2004, in Cosmic $\gamma$-ray Sources, ed. K. S. Cheng & G. E. Romero (Astrophysics and Space Science Library, Vol. 304; Dordrecht: Kluwer), 311
Nolan, P. L., Abdo, A. A., Ackermann, M., et al. (*Fermi*-LAT Collaboration) 2012, ApJS, 199, 31 (2FGL Catalog)
Nolan, P. L., Tompkins, W. F., Grenier, I. A., & Michelson, P. F. 2003, ApJ, 597, 615
Paredes, J. M., Martí, J., Ishwara-Chandra, C. H., et al. 2008, A&A, 482, 247
Plotkin, R., Anderson, S. F., Hall, P. B., et al. 2008, AJ, 135, 2453
Ransom, S. M., Ray, P. S., Camilo, F., et al. 2011, ApJ, 727, L16
Romani, R. W., & Shaw, M. S. 2011, ApJ, 743, L26
Saz Parkinson, P. M., Dormody, M., Ziegler, M., et al. 2010, ApJ, 725, 571
Skrutskie, M. F., Cutri, R. M., Stiening, R., et al. 2006, AJ, 131, 1163
Swanenburg, B. N., Bennett, K., Bignami, G. F., et al. 1981, ApJ, 243, L69
Takahashi, Y., Kataoka, J., Nakamori, T., et al. 2012, ApJ, 747, 64
Takeuchi, Y., Kataoka, J., Stawarz, Ł., et al. 2012, ApJ, 749, 66
Tavani, M., Mukherjee, R., Mattox, J. R., et al. 1997, ApJ, 479, L109
Teng, S. H., Mushotzky, R. F., Sambruna, R. M., Davis, D. S., & Reynolds, C. S. 2011, ApJ, 742, 66
Voges, W., Aschenbach, B., Boller, T., et al. 1999, A&A, 349, 389
Voges, W., Aschenbach, B., Boller, T., et al. 2000, IAU Circ., 7432, 3
Wolff, M. T., Wood, K. S., Abdo, A., et al. 2010, BAAS, 42, 669
Wright, E. L., Eisenhardt, P. R. M., Mainzer, A. K., et al. 2010, AJ, 140, 1868